
SECURING THE DARK MATTER: A SEMANTIC-ENHANCED NEURO-SYMBOLIC FRAMEWORK FOR SUPPLY CHAIN ANALYSIS OF OPAQUE INDUSTRIAL SOFTWARE

A PREPRINT

Bowei Ning^{1,2} **Xuejun Zong**^{2,3,*} **Lian Lian**^{2,3,*} **Kan He**^{2,3}
Yifei Sun^{2,3} Yuxiang Lei^{2,3} Plamen Vasilev⁴

¹School of Artificial Intelligence, Shenyang University of Technology, Shenyang 110870, China

²Key Laboratory of Information Security for Petrochemical Industry in Liaoning Province, Shenyang, China

³School of Information Engineering, Shenyang University of Chemical Technology, Shenyang 110142, China

⁴Department of Industrial Automation, University of Chemical Technology and Metallurgy, Sofia 1797, Bulgaria

*Corresponding authors: xuejun_zong@syuct.edu.cn; lianlian@syuct.edu.cn
Emails: 2020183@stu.syuct.edu.cn;

ABSTRACT

Automated vulnerability detection in critical-infrastructure software confronts a fundamental barrier: industrial software is routinely deployed as stripped, symbol-free binaries that deprive conventional Software Composition Analysis of the source-level transparency it requires. Existing binary analysis techniques close this Semantic Gap only partially—graph-based detectors preserve structural syntax but discard behavioral semantics, while large language models supply rich semantic cues at the cost of unstable, hallucination-prone inference. To address this gap, we present a semantic-enhanced neuro-symbolic framework that reconstructs behavioral semantics directly from opaque binaries and performs tractable global risk reasoning. Three tightly coupled mechanisms drive this capability: (1) abstract interpretation combined with a reflexive prompting pipeline that structurally constrains a local LLM agent, effectively suppressing hallucinations; (2) a surjective transformation that compresses raw Code Property Graphs into typed Software Supply Chain Knowledge Graphs amenable to scalable reasoning; and (3) a domain-adapted Graphormer that captures long-range vulnerability propagation, augmented by embedding-space subgraph matching to uncover zero-day and APT-style attack patterns. Evaluated across three benchmarks of increasing domain specificity, the framework consistently outperforms all baselines on detection accuracy, semantic lifting fidelity, and APT fingerprint matching. Deployment on a hybrid virtual-physical testbed incorporating production-grade hardware from five ICS vendors further confirms strong detection coverage of high-impact CVEs while substantially reducing false-positive rates relative to leading commercial tools. These results establish semantically grounded neuro-symbolic analysis as a tractable and effective approach to automated vulnerability assessment for opaque industrial software.

Keywords software supply chain security · knowledge graph · graph neural networks · large language models · vulnerability detection · opaque industrial software · binary analysis

1 Introduction

Modern software engineering has undergone a structural shift from monolithic development to component-based assembly. Developers routinely integrate hundreds of third-party libraries, producing deeply interdependent software supply chains. According to the 2024 Open Source Security and Risk Analysis report Synopsys, Inc. [2024], over 96% of codebases in the manufacturing and industrial sectors contain open-source components, a finding corroborated by the Linux Foundation’s Census III study Linux Foundation [2024]. However, this dependency network has significantly expanded the attack surface, allowing threats to migrate upstream. Adversaries no longer solely target hardened

production environments but increasingly infiltrate the development pipeline—tampering with source code or build environments—as evidenced by high-profile supply chain attacks such as SolarWinds and Log4j. Consequently, ensuring the transparency and traceability of the software supply chain has become a prerequisite for defense-in-depth architectures.

To mitigate these risks, the community has widely adopted Software Composition Analysis (SCA) and Software Bill of Materials (SBOM) tools to map known vulnerabilities Decan et al. [2019]. Nevertheless, these approaches rely heavily on the “transparency assumption”: the availability of source code, package manifests (e.g., `package.json`), or standard compilation metadata Liu et al. [2025]. Crucially, this assumption collapses when confronted with the Transparency Paradox inherent to critical infrastructure: regulators demand deep software visibility, yet vendors frequently deliver these systems as stripped, closed-source binaries Costin et al. [2016]. This paradox is especially severe in opaque industrial software—such as firmware used in aerospace, automotive, and Industrial Control Systems (ICS). Because this software relies on proprietary compilers (e.g., Tasking, Keil) and non-standard architectures, originally transparent open-source components devolve into opaque binary artifacts, rendering standard SCA tools completely ineffective Shoshitaishvili et al. [2016]. Bridging this opacity gap demands techniques that can recover semantic meaning directly from binary code—a requirement that the research community has only begun to address Yang et al. [2022].

Recent advances in automated vulnerability detection have yielded promising results on open-source codebases. Graph-based approaches such as Reveal Chakraborty et al. [2021] and SySeVR Li et al. [2021] capture structural dependencies via Code Property Graphs (CPG) and program slicing, while LLM-based approaches such as DeepSeek-Coder Guo et al. [2024] leverage pre-trained code models for semantic code understanding. Hybrid neuro-symbolic methods like GRACE Liu et al. [2023] integrate graph structure with LLM features to improve detection accuracy on standard benchmarks. However, these approaches have been developed and evaluated predominantly on source-level or open-source datasets and their applicability to stripped industrial binaries remains largely unexamined.

Bridging this opacity gap requires recovering semantic meaning directly from machine code. While deep learning has advanced open-source vulnerability detection, existing paradigms fail on opaque industrial binaries due to a profound ‘Semantic Gap’ Lin et al. [2020]. Specifically, traditional dynamic analysis and symbolic execution (e.g., angr) suffer from severe state explosion and hardware-emulation barriers when applied to monolithic firmware Muench [2019]. Graph Neural Networks (GNNs) capture structure via Code Property Graphs (CPGs) but treat stripped nodes as semantically hollow opcodes Chakraborty et al. [2021]. Conversely, Large Language Models (LLMs) offer semantic understanding but lack domain-specific industrial knowledge and are highly prone to hallucinating data-flow topologies when unconstrained by structural verifiers—a critical flaw that existing hybrid methods fail to address Wright et al. [2021].

To resolve this, we propose a semantic-enhanced neuro-symbolic framework that transforms opaque industrial binaries into computable Software Supply Chain Knowledge Graphs (SSCKGs). We conquer the semantic gap by formalizing the binary-to-semantics recovery as a Galois Connection between the concrete execution space and a domain-aware abstract security lattice (derived from MITRE ATT&CK). Unlike prior LLM-for-code approaches, we enforce this mapping via a Reflexive Prompting pipeline—a teacher-verifier-student loop—that utilizes structural graph verification to categorically reject LLM hallucinations.

This paper makes four principal contributions:

1. **Theoretically Grounded Semantic Lifting:** We instantiate the aforementioned Galois Connection using a three-tier, domain-aware abstract security lattice (comprising 5 macro-categories, 27 actions, and 43 risk labels) adapted from industrial standards. By executing the Reflexive Prompting pipeline, we fine-tune a 7B-parameter local agent that achieves a 94.2% empirical alignment (5.8% Empirical Violation Rate). This establishes a quantifiable soundness guarantee that is fundamentally absent from existing unconstrained LLM-for-code approaches.
2. **Knowledge Graph Compression and Risk Reasoning:** We design a surjective graph transformation (Φ) that overcomes the scalability limits of raw CPGs, compressing million-node structures into thousand-node SSCKGs governed by an eight-type vulnerability relation ontology. To perform risk reasoning, we introduce a domain-adapted Graphormer whose attention bias is modulated by semantic relation weights rather than mere topological distance, enabling it to capture the long-range dependency chains that standard message-passing GNNs consistently miss.
3. **Zero-Day and APT Fingerprinting via Embedding-Space Similarity:** To identify “legitimate-but-abnormal” logic hidden within opaque binaries, we propose a subgraph similarity algorithm operating directly in the Graphormer embedding space. Governed by a \mathcal{J} -optimal threshold that balances

detection sensitivity against operational alert fatigue, this module successfully detects zero-day threats and complex APT-level attack chains that evade traditional signature-based SCA tools.

4. **Comprehensive Evaluation on Opaque Industrial Software:** We conduct extensive experiments across three datasets of increasing domain specificity (Big-Vul, NVD-Precise, InduVul-Dataset) to validate the framework’s comparative efficacy and robustness. As a definitive case study, we deploy the system on a hybrid virtual–physical testbed utilizing production-grade hardware from 10 vendors; against 15 high-impact CVEs, the framework achieves a 93.3% detection rate while reducing the false-positive rate by 91.7% compared to leading commercial SCA tools.

The remainder of this paper is organized as follows. Section 2 surveys related work across graph-based, LLM-driven, and supply-chain-specific vulnerability detection. Section 3 formalizes the proposed framework: Semantic Lifting (Section 3.2), SCKG Construction (Section 3.3), Graphormer-based risk reasoning (Section 3.4), and APT Fingerprinting (Section 3.5). Section 4 presents the experimental evaluation across six research questions. Section 5 discusses implications, limitations, and threats to validity, followed by concluding remarks.

2 Related Work

We organize the related literature into four thematic areas: graph-based vulnerability detection, LLM-driven code understanding, industrial binary and firmware analysis, and code knowledge graphs. Table 1 at the end of this section provides a systematic comparison of representative approaches against five desiderata that motivate our framework.

2.1 Graph-Based Vulnerability Detection

Deep-learning-based vulnerability detection has progressed from sequence-oriented to graph-oriented representations. Early sequence-to-tensor methods such as VulDeePecker Li et al. [2018a] pioneered the application of deep learning to vulnerability detection by extracting local code gadgets and feeding them to bidirectional LSTMs. While this approach achieved promising results on controlled datasets, it inevitably discards the global execution topology — a limitation that subsequent graph-based methods sought to address.

SySeVR Li et al. [2021] advanced the field by combining syntax-based program slicing with Recurrent Neural Networks, capturing vulnerability-relevant code fragments along data- and control-dependence paths. Reveal Chakraborty et al. [2021] subsequently introduced Gated Graph Neural Networks (GGNNs) operating directly on Code Property Graphs (CPGs), aggregating AST, control-flow, and data-dependence information into a unified learned representation; on the Big-Vul benchmark, Reveal demonstrated significant improvements over prior sequence models. VulDecgre Dou et al. [2025] further exploited graph topology by transforming CPGs into centrality-based image representations for Convolutional Neural Networks.

Despite these advances, graph-based methods share two fundamental constraints when applied to stripped industrial binaries. First, they depend on the availability of source code or rich debug symbols to generate meaningful node attributes; when confronted with stripped firmware, nodes degenerate into generic opcode placeholders devoid of high-level semantic intent. Second, standard message-passing GNNs are inherently limited by their k -hop receptive field: in industrial supply chains, vulnerability propagation chains frequently span 10–15 hops (e.g., from a third-party library import to a sensitive write), a distance at which GNNs suffer from over-smoothing Li et al. [2018b]. Our framework addresses both limitations via Semantic Lifting (Section 3.2), which recovers behavioral semantics for stripped nodes, and a Graphormer architecture (Section 3.4), which captures global dependencies without the over-smoothing bottleneck.

2.2 LLM-Driven Code Understanding and Neuro-Symbolic Analysis

Large Language Models have substantially expanded the analytical capabilities available for code understanding. In the binary domain, BinLLM Pan et al. [2025] recovers variable names, function boundaries, and high-level summaries from raw assembly, while VulRepair Fu et al. [2022] applies T5-based sequence-to-sequence models to automated patch generation. Neuro-symbolic variants such as GRACE Liu et al. [2023] convert CPGs into prompts under a Retrieval-Augmented Generation loop, and PDBERT Liu et al. [2024] pre-trains a Transformer encoder on program dependency structures. These approaches share a common limitation: they treat the LLM as either a black-box oracle or a feature extractor, without any independent structural verification of its outputs, leaving hallucinations unbounded in principle.

The gap widens in the industrial domain, where generic LLMs lack knowledge of proprietary protocols and non-standard compiler artifacts, and consequently generate elevated false-positive rates on multi-component firmware. Our Reflexive

Prompting pipeline (Section 3.2.4) addresses this gap by introducing a structural oracle that rejects hallucinated data-flow edges before they enter the training corpus — a verification contract absent from prior hybrid methods.

2.3 Analysis of Opaque Industrial Firmware

Ensuring transparency across the industrial supply chain is a prerequisite for defense-in-depth. Emerging regulatory frameworks, including U.S. Executive Order 14028 National Institute of Standards and Technology [2021] and the NIST SP 800-82 guidelines National Institute of Standards and Technology [2023], mandate rigorous software supply chain transparency through mechanisms such as Software Bill of Materials (SBOM) generation. The IEC 62443 standard International Electrotechnical Commission [2013] further regulates secure product development lifecycles in ICS environments. In practice, industry tools such as Syft and Trivy map component dependencies by parsing package manifests. This regulatory push creates the aforementioned Transparency Paradox: while standards demand deep visibility, industrial vendors frequently deliver opaque, closed-source firmware that lacks the package manifests (e.g., `package.json`, `conanfile.txt`) on which existing SCA tools depend.

On the analysis side, efforts to penetrate this opacity have encountered severe architectural bottlenecks. Static and symbolic execution platforms `angr` Shoshitaishvili et al. [2016] face well-documented scalability limits when applied to monolithic firmware. While formal verification has been proposed for Programmable Logic Controller (PLC) programs Zhang et al. [2024], such approaches assume access to structured ladder-logic source code—an assumption that fails for stripped binaries. Conversely, dynamic analysis techniques, including firmware fuzzers Srivastava et al. [2019] and runtime monitors Tan et al. [2026], hit the ‘Environment Wall’ Muench [2019]: emulating proprietary hardware peripherals for high-coverage dynamic testing remains prohibitively expensive and often impractical Wright et al. [2021].". Our SSCKG construction (Section 3.3) resolves this impasse. By operating entirely on static binary artifacts, it bypasses the hardware-emulation barrier of dynamic analysis, while simultaneously recovering the high-level behavioral semantics that traditional static tools discard.

2.4 Code Representation and Software Knowledge Graphs

Because transforming the CPG into the SSCKG is a primary methodological contribution of this work (Section 3.3), it is important to position it against existing code knowledge graphs. CodeQL Youn et al. [2023], developed by GitHub, maps source-level ASTs into a relational database and supports Datalog-style semantic queries; it excels at pattern-based vulnerability detection for open-source projects but operates exclusively on source code and lacks abstract semantic or risk-propagation reasoning. Developer-centric knowledge graphs such as DevKG link pull requests, commits, and developer metadata to facilitate project-level analytics, yet they encode no behavioral semantics of the code itself. More recent work on code knowledge graphs has explored embedding function-level summaries as node attributes, but these graphs remain anchored to source-level identifiers and do not generalize to stripped binaries.

In contrast, our SSCKG is an *abstracted behavioral graph* specifically designed for opaque firmware. It differs from the above in three respects: (1) entities are elevated from instruction-level CPG nodes to behaviorally typed units via the Semantic Lifting stage, enabling analysis of stripped binaries without source code; (2) relations encode multi-hop vulnerability propagation paths (e.g., `taints`, `reaches`) drawn from a formal eight-type ontology (Table 2), rather than raw syntactic edges; and (3) the surjective transformation Φ (Section 3.3) provides a principled compression from millions of instruction-level nodes to thousands of semantically meaningful entities, making downstream Graphormer reasoning tractable.

2.5 Summary and Positioning

The preceding review reveals a consistent pattern: graph-based methods offer structural rigor but lack semantic depth for stripped binaries; LLM-based methods provide semantic insight but lack structural grounding and domain specificity; industrial analysis tools face hardware-emulation barriers; and existing code knowledge graphs do not generalize beyond source-level representations. Table 1 synthesizes these observations across five desiderata.

To the best of our knowledge, no existing work integrates LLM-driven abstract interpretation with Graphormer-based graph reasoning to construct a formally grounded, verifiable knowledge graph for the opaque industrial software supply chain. The proposed framework addresses this gap through four complementary mechanisms: a Galois Connection that provides soundness guarantees for LLM-based semantic recovery (Section 3.2), a Reflexive Prompting pipeline that eliminates hallucinated abstractions (Section 3.2.4), a surjective SSCKG transformation that encodes vulnerability propagation semantics (Section 3.3), and a domain-adapted Graphormer that captures long-range dependency chains beyond the reach of standard GNNs (Section 3.4).

Table 1: Comparison of representative approaches against five desiderata for industrial supply chain vulnerability detection. \checkmark = fully addressed; \triangle = partially addressed; \times = not addressed.

Approach	Structural Analysis	Semantic Understanding	Industrial Domain	Binary Ready	Formal Guarantee
VulDeePecker Li et al. [2018a]	\times	\times	\times	\times	\times
SySeVR Li et al. [2021]	\checkmark	\times	\times	\times	\times
Reveal Chakraborty et al. [2021]	\checkmark	\times	\times	\times	\times
DeepSeek-Coder Guo et al. [2024]	\times	\checkmark	\times	\triangle	\times
GRACE Liu et al. [2023]	\checkmark	\checkmark	\times	\times	\times
CodeQL Youn et al. [2023]	\checkmark	\triangle	\times	\times	\times
angr Shoshitaishvili et al. [2016]	\checkmark	\times	\triangle	\checkmark	\times
Ours	\checkmark	\checkmark	\checkmark	\checkmark	\checkmark

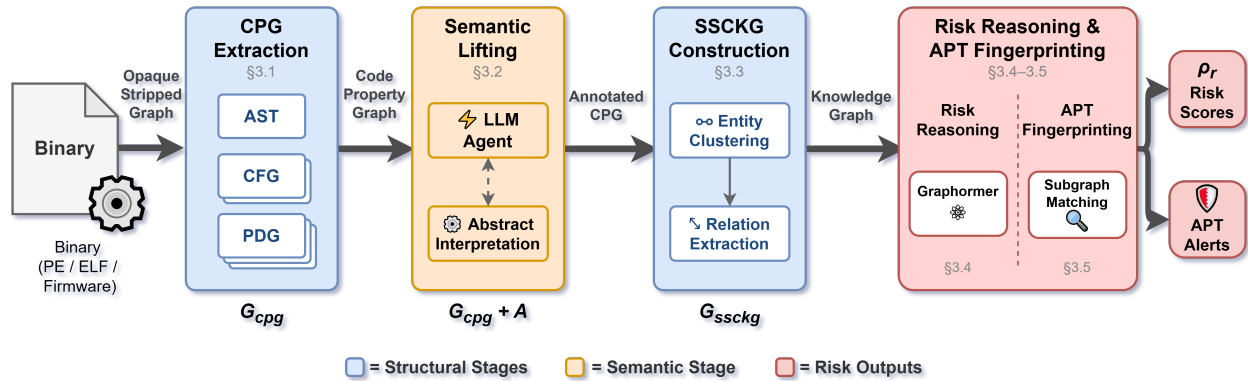


Figure 1: End-to-end pipeline of the proposed SCAA framework. A stripped binary is first parsed into a Code Property Graph (G_{cpg} , Section 3.1), then semantically lifted via a teacher–verifier–student loop (Section 3.2). The annotated CPG is transformed into a Software Supply Chain Knowledge Graph (G_{ssckg} , Section 3.3), on which a domain-adapted Graphormer performs risk reasoning and APT fingerprinting (Sections 3.4–3.5). Color coding: blue for structural stages, orange for semantic stages, red for risk outputs.

3 Methodology

3.1 Preliminaries and Problem Formulation

The fundamental challenge in auditing the industrial software supply chain is the absence of source code and debug symbols. To systematically analyze these opaque binaries, our Supply Chain Analysis Agent (SCAA) first parses the target executable (e.g., PE/ELF files or firmware images) into a structural representation.

Pipeline Overview. To address the semantic gap inherent in stripped binaries, we propose an end-to-end neuro-symbolic workflow comprising four sequential stages (illustrated in Figure 1):

1. **Binary** \rightarrow **CPG Extraction** (Section 3.1): The executable is parsed into a Code Property Graph that unifies AST, CFG, and PDG representations.
2. **Semantic Lifting** (Section 3.2): A fine-tuned LLM agent, governed by Abstract Interpretation theory, maps low-level instructions to a hierarchical domain of opaque industrial software security behaviors.
3. **SSCKG Construction** (Section 3.3): The annotated CPG is transformed into a compact Knowledge Graph with typed vulnerability relations via entity clustering and relation extraction.
4. **Risk Reasoning & APT Fingerprinting** (Sections 3.4–3.5): A domain-adapted Graphormer captures long-range dependency chains and computes composite risk scores; a subgraph similarity algorithm detects zero-day threats by matching against known APT behavioral fingerprints.

Code Property Graph (CPG): We adopt the standard CPG formalism Yamaguchi et al. [2014] as our foundational data structure because it integrates Abstract Syntax Trees (AST), Control Flow Graphs (CFG), and Program Dependence

Graphs (PDG) into a single queryable multigraph $G_{cpg} = (V, E)$ with edge set $E = E_{ast} \cup E_{cfg} \cup E_{pdg}$, where nodes carry opcode and type attributes and edges carry structural or data-flow labels — a unification essential for tracking cross-component vulnerabilities.

The Semantic Gap Problem: While G_{cpg} mathematically captures the topology of execution paths and data dependencies, it inherently lacks high-level behavioral semantics when generated from stripped binaries. A subgraph representing a proprietary industrial compiler operation or a hardware-controller state-machine translation remains semantically opaque; standard graph traversal algorithms cannot differentiate between a legitimate network initialization and a malicious backdoor connection based purely on structural features.

Problem Formulation: We formulate the task of Industrial Supply Chain Vulnerability Detection as a two-stage neuro-symbolic learning problem. Given a stripped binary artifact \mathcal{B} , our ultimate objective is to learn a risk prediction function $\mathcal{F} : \mathcal{B} \rightarrow [0, 1]$. Because direct mapping is intractable due to the aforementioned semantic gap, we decompose \mathcal{F} into two distinct operations:

1. **Semantic Transformation (Φ):** We must define a mapping function that elevates the structurally rigid but semantically sparse G_{cpg} into a rich, queryable Software Supply Chain Knowledge Graph (SSCKG), representing “behavior-dependency-risk” relationships.
2. **Risk Reasoning (Ψ):** We must define a graph reasoning function operating on the SSCKG to capture multi-hop, long-range dependencies and output a composite risk score ρ_r , enabling the detection of both known components and zero-day anomalous behaviors.

Concretely, Φ is realized across Sections 3.2–3.3: the Semantic Lifting stage (Section 3.2) maps concrete binary instructions onto abstract behavioral labels in \mathcal{A} , while the SSCKG Construction stage (Section 3.3) compresses those annotated instructions into a compact, typed knowledge graph G_{ssckg} . The Risk Reasoning function Ψ is then realized in Sections 3.4–3.5, which operate jointly on G_{ssckg} to produce composite risk scores and zero-day alert decisions. The following subsections detail each stage in sequence. All non-standard symbols are introduced inline on first use.

3.2 Semantic Lifting via Abstract Interpretation

To bridge the semantic gap inherent in stripped binaries, we propose a Semantic Lifting approach governed by the theory of Abstract Interpretation. Unlike traditional pattern-matching techniques (e.g., YARA rules or byte-signature scanners) that fail on obfuscated or previously unseen code, we model the semantic recovery process as a principled mapping between the concrete execution space of the binary and an abstract security domain. This formulation provides a theoretical foundation for quantifying the fidelity of LLM-based code understanding — a guarantee absent from existing LLM-for-code approaches that treat the model as a black-box oracle.

3.2.1 Abstract Domain Definition

Let \mathcal{C} denote the concrete state space of the program (registers and memory) and \mathcal{A} denote the abstract domain representing high-level security behaviors. We define \mathcal{A} as a finite, domain-aware hierarchical lattice representing high-level security behaviors in opaque industrial software. To instantiate this lattice for our primary ICS case study, we derive the specific behavioral labels from the MITRE ATT&CK for ICS matrix MITRE Corporation [2024]; other domains would substitute domain-appropriate label sets while preserving the same three-tier structure. The hierarchy is organized as follows:

- **Tier 1 (Macro-Behavior):** Five root categories — Network, Memory, Hardware, FileSystem, and Cryptography.
- **Tier 2 (Specific Action):** Fine-grained behavioral labels within each category. For example, Network decomposes into Socket_Init, Protocol_Parse, DNS_Resolve; Hardware includes Register_Read, Coil_Write, Firmware_Update.
- **Tier 3 (Risk Context):** Security-qualified variants that encode violation conditions, e.g., Unauthenticated_Coil_Write, Unbounded_Protocol_Parse.

In total, \mathcal{A} comprises 5 macro-categories, 27 specific actions, and 43 risk-contextualized labels. The partial order \sqsubseteq on \mathcal{A} follows the containment hierarchy: a Tier 3 label is below its parent Tier 2 action, which is below its Tier 1 category, with \top denoting the universal “Unknown Behavior” element. This lattice structure ensures that over-approximation (mapping to a coarser category) preserves soundness, while under-approximation (missing a risk context) constitutes a violation. Figure 2 depicts representative branches of this three-tier lattice, illustrating how concrete binary behaviors are progressively abstracted into security-relevant categories.

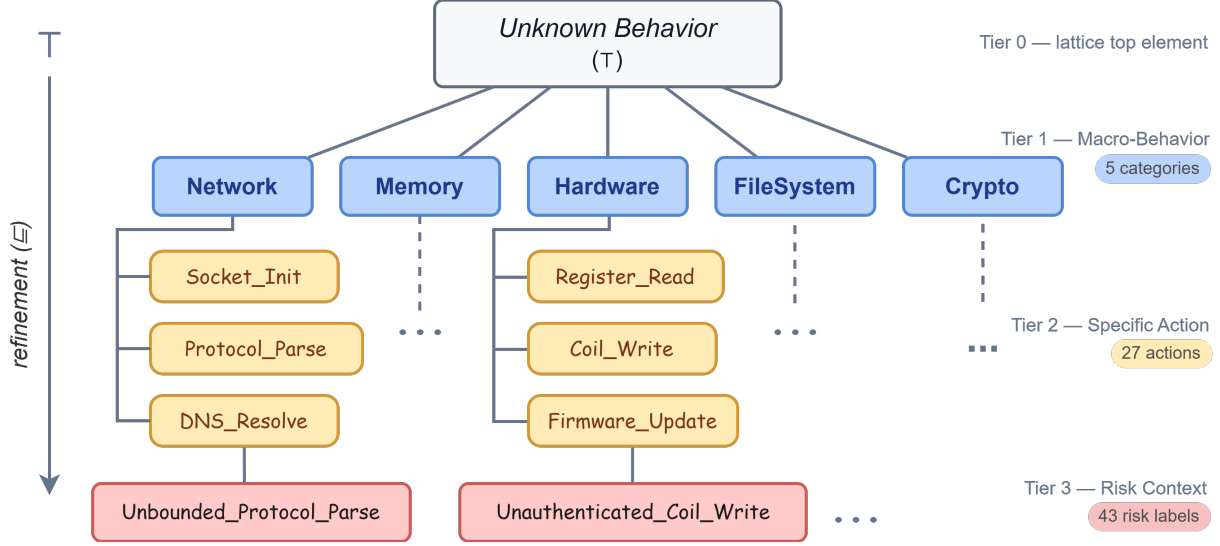


Figure 2: Three-tier abstract domain \mathcal{A} derived from MITRE ATT&CK for ICS. Tier 1 comprises 5 macro-behavior categories; Tier 2 refines these into 27 specific actions; Tier 3 qualifies 43 risk-contextualized labels. The partial order \sqsubseteq follows the containment hierarchy, with \top (Unknown Behavior) as the top element. Only representative branches are shown for clarity.

3.2.2 Galois Connection Formulation

We establish a Galois Connection (α, γ) Cousot and Cousot [1977] between the concrete and abstract spaces:

$$\alpha : \mathcal{P}(\mathcal{C}) \rightarrow \mathcal{A}, \quad \gamma : \mathcal{A} \rightarrow \mathcal{P}(\mathcal{C}) \tag{1}$$

where α is the abstraction function and γ is the concretization function. The pair (α, γ) constitutes a valid Galois Connection if and only if $\alpha(c) \sqsubseteq a \iff c \in \gamma(a)$ for all $c \in \mathcal{P}(\mathcal{C})$ and $a \in \mathcal{A}$ Cousot and Cousot [1977]. Because the concrete state space \mathcal{C} (registers and memory) is unbounded, $\gamma(a)$ is not computationally tractable. Compounding this, the concrete transition function F (the binary execution) is opaque for stripped binaries, making $\alpha \circ F$ inaccessible. We therefore employ a Large Language Model (LLM) agent, specifically a fine-tuned Qwen3-7B Yang et al. [2025] (via QLoRA Dettmers et al. [2023]), to approximate the abstract transition function F^\sharp . The objective is to ensure that the LLM’s interpretation satisfies the soundness condition:

$$\alpha(F(c)) \sqsubseteq F^\sharp(\alpha(c)) \tag{2}$$

where \sqsubseteq represents the partial order in the risk hierarchy defined above. Intuitively, this condition requires that the LLM’s behavioral summary must *cover* the true concrete behavior — it may over-approximate (e.g., labeling a benign function as `Network` when only `Socket_Init` applies) but must not *miss* security-relevant behaviors.

3.2.3 Empirical Soundness Verification

Due to the probabilistic nature of LLMs, absolute mathematical soundness is intractable. We instead define the *Empirical Violation Rate* (EVR, formally stated in Eq. 10, Section 4.2.3) as the fraction of curated Golden Set functions whose LLM-predicted abstract label fails to cover the expert ground truth in the lattice \mathcal{A} . A lower EVR indicates that the approximation F^\sharp is closer to the ideal abstraction function. The full empirical validation — including per-category breakdown, error taxonomy, and comparison against baseline LLMs — is reported in Section 4.4 (RQ4).

3.2.4 Reflexive Prompting: A Teacher–Student Verification Loop

To minimize the EVR and enforce structural consistency, the SCAA employs a Reflexive Prompting mechanism comprising a teacher–student pipeline with graph-based verification. Unlike standard knowledge distillation, this loop incorporates a structural oracle (the Joern CPG server Yamaguchi et al. [2014]) as an independent verifier, ensuring that the LLM’s semantic summaries remain grounded in the program’s actual data-flow topology.

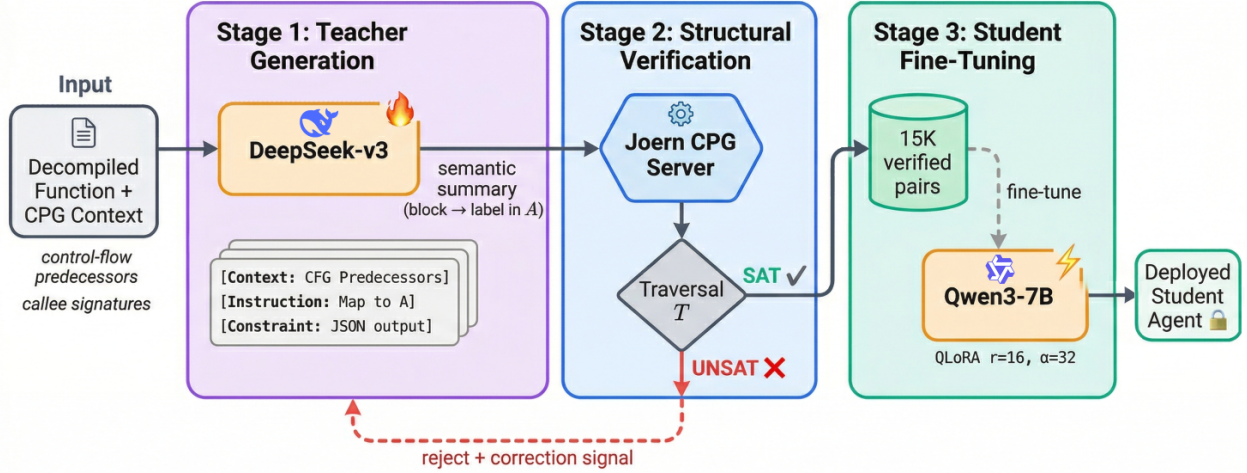


Figure 3: Reflexive Prompting pipeline. The teacher model (DeepSeek-v3) generates semantic summaries, which are verified against the CPG by the Joern structural oracle. Summaries that fail the SAT check (15.8% rejection rate) are discarded. The 15,000 verified instruction–behavior pairs are used to fine-tune the student model (Qwen3-7B) via QLoRA (rank=16, $\alpha=32$, lr= 2×10^{-4} , 5 epochs).

The procedure operates as follows:

1. **Teacher Generation:** A large-capacity teacher model (DeepSeek-v3) receives a decompiled function along with its CPG context (control-flow predecessors, callee signatures) and produces an initial semantic summary, mapping each basic block to a label in \mathcal{A} . The prompt template follows a structured format: [Context: Control Flow Predecessors], [Instruction: Map to Domain \mathcal{A}], [Constraint: Output strict JSON].
2. **Structural Verification:** The Joern server executes a graph traversal T based on the teacher’s claimed data-flow paths. If the traversal returns UNSAT (i.e., the teacher hallucinated a data-flow edge that does not exist in the CPG), a negative correction signal is generated, and the teacher’s summary is rejected for that block.
3. **Student Fine-Tuning:** The structurally verified summaries form a training corpus of 15,000 instruction–behavior pairs. We fine-tune the local Qwen3-7B agent via QLoRA (rank 16, $\alpha=32$) with a learning rate of 2×10^{-4} . Training was halted after 5 epochs when validation loss plateaued at 0.12.

This three-stage pipeline ensures that the student model inherits the teacher’s broad semantic understanding while the structural verifier eliminates hallucinated abstractions that violate the CPG’s ground-truth topology. We select Qwen3-7B as the student model for its strong performance on code understanding benchmarks while remaining deployable on a single GPU (24 GB VRAM) — a practical requirement for offline industrial environments where cloud API access is restricted. Figure 3 summarizes the complete teacher–verifier–student loop, including the rejection rate and key training hyperparameters.

The verified $\langle f_i, \ell_T \rangle$ pairs produced by the fine-tuned student model M_S^* constitute the behavioral annotations that seed both downstream stages: the abstract labels in \mathcal{A} drive entity clustering in Section 3.3, and the behavioral summaries $\text{desc}(v)$ feed the inherent risk computation $\rho_{\text{inherent}}(v)$ in Section 3.4 (Eq. 8).

3.3 SSCKG Construction: The Semantic Graph Transformation

With each basic block now annotated with behavioral labels from \mathcal{A} , the next stage transforms the fine-grained CPG into a compact, queryable Software Supply Chain Knowledge Graph (SSCKG). This transformation serves two purposes: it reduces the graph from millions of instruction-level nodes to thousands of semantically meaningful entities, and it introduces typed relations that encode vulnerability propagation paths not explicit in the original CPG. We formalize this as a surjective graph transformation function Φ :

Algorithm 1: Reflexive Prompting Corpus Construction

Input: Function set $\mathcal{F} = \{f_i\}$; CPG oracle JOERN; teacher model M_T (DeepSeek-v3); student model M_S (Qwen3-7B)

Output: Fine-tuned student model M_S^*

```

1  $\mathcal{D} \leftarrow \emptyset$ 
2 foreach  $f_i \in \mathcal{F}$  do
3    $\ell_T \leftarrow M_T(f_i, \text{CPG\_CONTEXT}(f_i))$  // Teacher: generate semantic summary
4    $r \leftarrow \text{JOERN.TRAVERSE}(f_i, \ell_T.\text{data\_flow\_claims})$  // Verifier: check structural consistency
5   if  $r \neq \text{UNSAT}$  then
6      $\mathcal{D} \leftarrow \mathcal{D} \cup \{(f_i, \ell_T)\}$  // Accept verified pair ( $\approx 84.2\%$  of inputs)
7   end
8   else
9     discard  $\ell_T$  // Reject hallucinated data-flow edges (15.8%)
10  end
11 end
12  $M_S^* \leftarrow \text{QLORA\_FINETUNE}(M_S, \mathcal{D}, \text{rank}=16, \alpha=32, \text{lr}=2 \times 10^{-4}, \text{epochs}=5)$ 
13 return  $M_S^*$ 

```

$$\Phi : G_{\text{cpg}}(V, E) \rightarrow G_{\text{ssckg}}(\mathcal{E}, \mathcal{R}) \quad (3)$$

We note that Φ is *not* an isomorphism: it deliberately introduces semantic information (behavioral labels, risk relations) that is absent in the source CPG, while collapsing structurally redundant nodes. The transformation consists of two concurrent processes.

3.3.1 Entity Elevation ($\Phi_{\mathcal{E}}$)

Nodes $v \in V$ in the CPG are clustered and mapped to high-level entities $e \in \mathcal{E}$ via a hybrid algorithm that combines structural boundaries with semantic similarity:

1. **Structural Collapse (Rule-Based):** All AST nodes belonging to a single basic block or a single function body are collapsed into one entity e_i . This step preserves program structure boundaries and reduces the node count by approximately two orders of magnitude, following standard program slicing conventions Korel and Rilling [1998].
2. **Semantic Clustering (Embedding-Based):** For external library calls and cross-module functions, we generate Sentence-BERT Reimers and Gurevych [2019] embeddings of the behavioral summaries produced by the Semantic Lifting stage (Section 3.2). We then apply DBSCAN Ester et al. [1996] ($\epsilon=0.3$, $\text{min_samples}=2$) to cluster semantically equivalent but syntactically distinct functions. For example, `s7_read_req` and `read_modbus_register` — despite having different implementations — both cluster into the entity `PLC_Read_Request` (the ICS-domain label for this behavioral class; analogous entity names would apply in automotive or aerospace instantiations), because their behavioral summaries share the Tier 2 label `Register_Read`. We select DBSCAN over k -means because the number of semantic clusters is not known a priori and DBSCAN naturally identifies noise points (functions with unique behaviors).

3.3.2 Relation Extraction ($\Phi_{\mathcal{R}}$)

Edges in the CPG are transformed into semantically typed relations. We define a relation ontology $\Sigma_{\mathcal{R}}$ comprising eight relation types organized into three categories, summarized in Table 2.

The eight-relation ontology was derived by cross-mapping the tactic categories of MITRE ATT&CK against the CWE vulnerability taxonomy from the NVD. Each of the three structural relations corresponds to a CPG edge type; each data-flow relation encodes a program dependence direction; and the three vulnerability relations cover the full spectrum from upstream taint propagation to direct CVE matching. Relations outside the scope of device-level opaque software execution — such as multi-node network topology links or high-level session states — are intentionally excluded and constitute a known limitation acknowledged in Section 5.2.

Relation types are assigned deterministically: structural relations are inherited directly from the CPG edge types (E_{ast} , E_{cfg}); data-flow relations are derived from E_{pdg} edges; and vulnerability relations are inferred by combining the

Table 2: SSCKG Relation Ontology ($\Sigma_{\mathcal{R}}$). Eight typed relations in three categories, with their derivation source from the CPG edge sets.

Category	Relation Type	Source	Semantics
Structural	calls	E_{ast}	Function invocation
	depends_on	E_{ast}	Build/link dependency
	imports	E_{ast}	Library inclusion
Data Flow	reads_from	E_{pdg}	Memory/register read
	writes_to	E_{pdg}	Memory/register write
Vulnerability	taints	$E_{pdg} + \text{NVD}$	Tainted data propagation
	reaches	$E_{pdg} + \text{NVD}$	Reachability to sensitive op
	vulnerable_to	NVD match	Entity \rightarrow CVE mapping

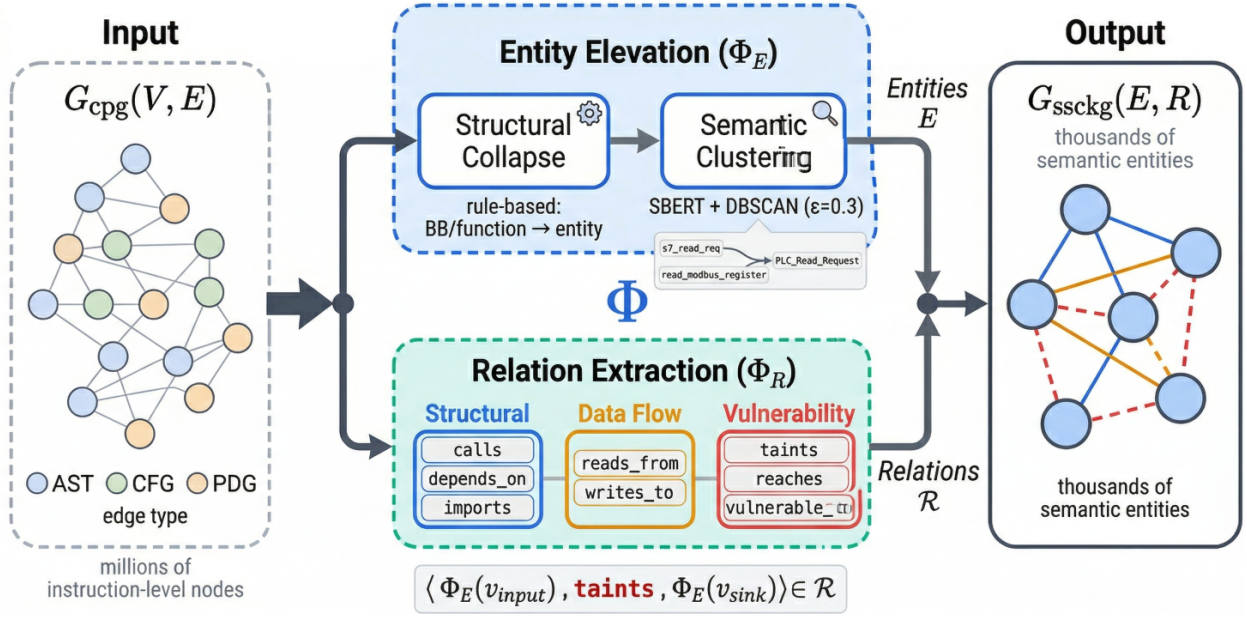


Figure 4: Concrete example of the surjective transformation $\Phi : G_{cpg} \rightarrow G_{ssckg}$. **Left:** A CPG fragment (~ 20 nodes) from a Modbus protocol handler, with AST (solid), CFG (dashed), and PDG (dotted) edges. **Right:** The resulting SSCKG fragment (~ 5 entities) after Entity Elevation and Relation Extraction, showing typed relations from $\Sigma_{\mathcal{R}}$ (Table 2). Arrows indicate which CPG nodes collapse into each SSCKG entity; for instance, `s7_read_req` and `read_modbus_register` cluster into `PLC_Read_Request`.

Semantic Lifting labels with known vulnerability patterns from the NVD. For instance, a data dependency edge e_{pdg} connecting a user input node to a sensitive API node is transformed into a risk relation triplet:

$$r_{flow} = \langle \Phi_{\mathcal{E}}(v_{input}), \text{taints}, \Phi_{\mathcal{E}}(v_{sink}) \rangle \in \mathcal{R} \quad (4)$$

This typed relation ontology distinguishes our SSCKG from generic code knowledge graphs (e.g., those constructed by CodeQL Youn et al. [2023]), which lack explicit vulnerability propagation semantics. To make this transformation concrete, Figure 4 presents a before-and-after example showing how a CPG fragment is compressed and enriched into an SSCKG subgraph with typed vulnerability relations.

The resulting $G_{ssckg}(\mathcal{E}, \mathcal{R})$ is the sole input consumed by both subsequent stages: Section 3.4 uses its entity set \mathcal{E} and typed relations \mathcal{R} to drive Graphormer attention and composite risk scoring, while Section 3.5 matches subgraphs of G_{ssckg} against APT fingerprints in embedding space.

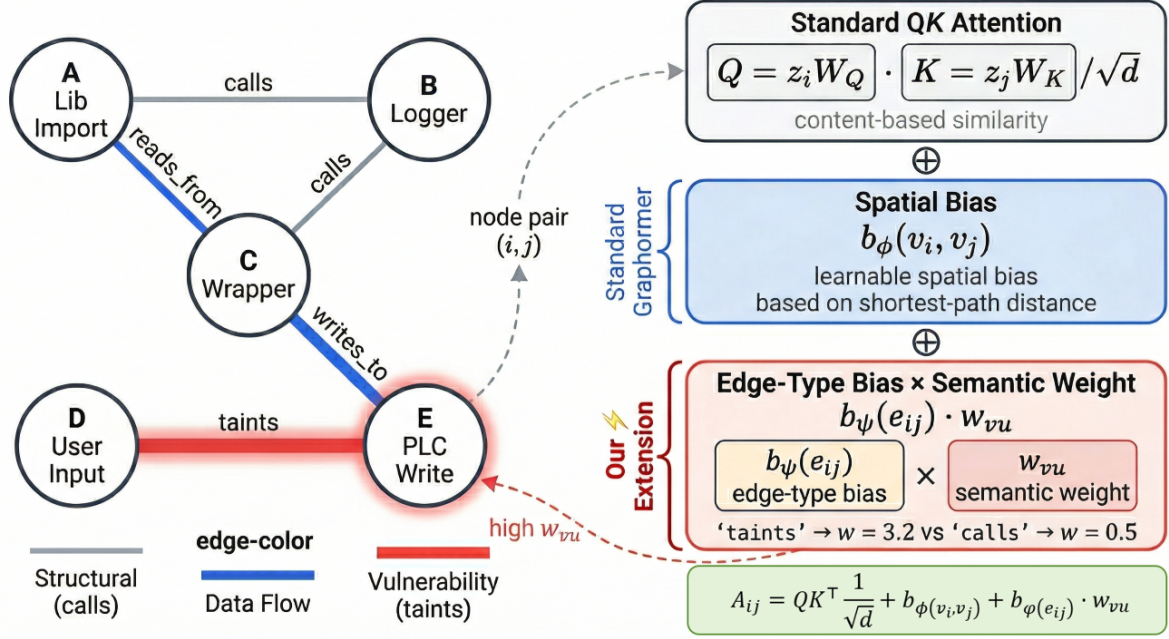


Figure 5: Domain-specific attention bias in a single Graphormer head. **Top:** Standard Graphormer biases attention by shortest-path distance b_ϕ only. **Bottom:** Our extension adds an edge-type bias b_ϕ modulated by the semantic weight w_{vu} from $\Sigma_{\mathcal{R}}$, amplifying vulnerability-relevant paths (taints, reaches) over structural edges (calls, imports). Edge colors encode relation type; line thickness reflects attention magnitude.

3.4 Graph Representation Learning via Graphormer

With the SCKG constructed, the next stage identifies latent risks by capturing complex, non-local dependencies between entities. As discussed in Section 2.1, message-passing GNNs suffer from k -hop receptive fields and over-smoothing Li et al. [2018b] when propagation chains span 10–15 hops, as is common in industrial supply chains. To overcome this limitation, we employ a Graphormer architecture Ying et al. [2021]. Unlike message-passing GNNs, Graphormer utilizes a Transformer-based global attention mechanism, allowing every node to attend to every other node in a single layer, regardless of topological distance. This architectural choice is motivated by the observation that vulnerability propagation in supply chains is fundamentally a *global* property: a compromised upstream library affects all downstream consumers, irrespective of their position in the call graph.

The node update rule for the l -th layer follows the standard Graphormer formulation:

$$\mathbf{z}_v^{(l+1)} = \text{LayerNorm}\left(\mathbf{z}_v^{(l)} + \text{FFN}\left(\text{MultiHeadAttn}(\mathbf{z}^{(l)})\right)\right) \quad (5)$$

3.4.1 Domain-Specific Edge Encoding

While Eq. 4 is the standard Graphormer update, our key adaptation lies in the attention bias computation. In the original Graphormer Ying et al. [2021], the attention score A_{ij} is biased solely by the shortest-path distance $\phi(v_i, v_j)$. We extend this by modulating the bias with the *semantic weight* w_{vu} of the edge, derived from the relation ontology $\Sigma_{\mathcal{R}}$ defined in Section 3.3:

$$A_{ij} = \frac{(\mathbf{z}_i \mathbf{W}_Q)(\mathbf{z}_j \mathbf{W}_K)^\top}{\sqrt{d}} + b_\phi(v_i, v_j) + b_\phi(e_{ij}) \cdot w_{vu} \quad (6)$$

Figure 5 contrasts the standard Graphormer attention bias (spatial only) with our extended formulation, illustrating how edge-type and semantic weight jointly modulate the attention scores on a representative SCKG subgraph.

Here, b_ϕ is the learnable spatial bias and b_ϕ is the learnable edge-type bias. The semantic weight w_{vu} is assigned based on relation type: a taints edge connecting user input to a PLC hardware interrupt receives a substantially higher

attention bias than a calls edge between two benign logging functions. This domain-specific weighting ensures that the model prioritizes vulnerability-relevant paths during attention computation, rather than treating all graph edges uniformly.

3.4.2 Composite Risk Score

Based on the learned node embeddings \mathbf{z}_v , we compute the Composite Risk Score $\rho_r(v)$ for each entity. This score aggregates both the inherent vulnerability of the node and the contextual risk propagated from its neighbors:

$$\rho_r(v) = \beta \cdot \rho_{\text{inherent}}(v) + (1 - \beta) \cdot \frac{1}{|\mathcal{N}(v)|} \sum_{u \in \mathcal{N}(v)} w_{vu} \cdot \rho_r(u) \quad (7)$$

Eq. 7 is solved via power iteration: beginning from $\rho_r^{(0)}(v) = \rho_{\text{inherent}}(v)$, each step updates all entity scores simultaneously until $\|\rho_r^{(t+1)} - \rho_r^{(t)}\|_1 < 10^{-6}$ (typically 20–30 iterations). Convergence is guaranteed by the Perron–Frobenius theorem provided the weight matrix $W = \{w_{vu}\}$ is row-stochastic after per-node normalization, which our relation-weight assignment satisfies by construction. We further note that Eq. 7 structurally resembles Personalized PageRank Bianchini et al. [2005] with ρ_{inherent} serving as the personalization vector. This connection is deliberate: PageRank’s iterative diffusion naturally models how risk propagates through dependency chains, while the learned attention weights w_{vu} from the Graphormer replace the uniform transition probabilities with semantically informed edge strengths.

The inherent risk $\rho_{\text{inherent}}(v)$ is computed via Sentence-BERT Reimers and Gurevych [2019] semantic alignment between the entity’s behavioral summary (from Section 3.2) and known CVE descriptions from the NVD (the same Sentence-BERT encoder used for behavioral clustering in Section 3.3.1; embeddings are computed once during SSCKG construction and reused here without recomputation). Specifically:

$$\rho_{\text{inherent}}(v) = \max_{c \in \text{CVE}_{\text{ICS}}} \cos(\text{SBERT}(\text{desc}(v)), \text{SBERT}(\text{desc}(c))) \quad (8)$$

where $\text{desc}(v)$ is the Semantic Lifting summary of entity v and $\text{desc}(c)$ is the textual description of CVE entry c . The damping factor β is set to 0.15, following the standard PageRank convention, and validated via grid search on the development set (Section 4).

The Graphormer node embeddings \mathbf{z}_v produced by this stage serve a dual role: the composite risk scores $\rho_r(v)$ drive the vulnerability detection decisions reported in Section 4, while the embedding vectors themselves are passed directly to the APT fingerprinting module in Section 3.5, where cosine similarity in embedding space replaces intractable structural subgraph isomorphism.

3.5 Zero-Day Threat Detection via APT Fingerprinting

The preceding stages address known (1-day) vulnerability detection. However, a critical requirement for industrial security is the detection of Advanced Persistent Threats (APTs) and zero-day exploits that utilize “legitimate but abnormal” logic — for instance, a specific sequence of PLC register writes combined with a covert network socket opening — that evades standard signature-based detection.

We formulate this as a Subgraph Similarity Search problem operating in the Graphormer embedding space, rather than on raw graph structure. This design choice is motivated by a key observation: while structural subgraph isomorphism is NP-hard in general Cordella et al. [2004], computing cosine similarity between fixed-dimensional embeddings is $O(|\mathcal{V}_{\text{apt}}| \cdot |\mathcal{V}_{\text{target}}|)$, which is tractable for the entity-level SSCKG (typically 10^3 – 10^4 nodes after Entity Elevation).

3.5.1 APT Fingerprint Construction

We maintain a repository of APT Fingerprints, represented as abstract subgraphs \mathcal{G}_{apt} , constructed via a semi-automated extraction pipeline:

1. **Source Data:** To model advanced threats targeting opaque industrial software, we utilize the MITRE Engenuity ICS APT evaluation dataset. This provides documented behavioral traces for sophisticated supply chain and logic-level attacks (e.g., Stuxnet, Triton, and HAVEX). MITRE Engenuity [2023].
2. **SSCKG Generation:** Known malware binaries are processed through the full SCAA pipeline (Sections 3.2–3.4) to generate their SSCKGs, producing entity-level behavioral graphs with typed relations.

3. **Expert Pruning:** Since malware SSCKGs contain substantial boilerplate code (e.g., runtime initialization, benign library calls), domain experts manually pruned each graph to isolate the core malicious subgraphs \mathcal{G}_{apt} . For example, the Stuxnet fingerprint retains only the subgraph where a malicious DLL injection leads to rogue `s7comm` packets targeting specific PLC models, discarding unrelated system initialization routines.

3.5.2 Similarity Metric

To detect a potential zero-day threat, we compute the semantic similarity between the target software’s SSCKG $\mathcal{G}_{\text{target}}$ and each fingerprint in the repository. The metric is defined as the average best-match cosine similarity:

$$\text{Sim}(\mathcal{G}_{\text{target}}, \mathcal{G}_{\text{apt}}) = \frac{1}{|\mathcal{V}_{\text{apt}}|} \sum_{v \in \mathcal{V}_{\text{apt}}} \max_{u \in \mathcal{V}_{\text{target}}} \cos(\mathbf{z}_u, \mathbf{z}_v) \quad (9)$$

where \mathbf{z}_u and \mathbf{z}_v are the Graphormer embeddings from Section 3.4. We adopt this asymmetric formulation (averaging over the fingerprint, maximizing over the target) because an APT fingerprint captures a *necessary* behavioral pattern: every node in the fingerprint must find a semantic match in the target, but the target may contain additional benign functionality. This design is robust against code obfuscation because it operates on semantic embeddings rather than raw structural features, allowing the system to identify functionally equivalent attack patterns even when the underlying binary implementation varies.

3.5.3 Threshold Determination

The alert threshold τ_{apt} is not a manually tuned constant. We determine τ_{apt} empirically via grid search on the validation splits of the Big-Vul and InduVul datasets, optimizing Youden’s J statistic ($J = \text{TPR} - \text{FPR}$) Youden [1950] on the ROC curve. This criterion maximizes the True Positive Rate (recall for zero-day threats) while strictly constraining the False Positive Rate to $\leq 5\%$, a requirement driven by the operational reality that high FPR causes “alert fatigue” in industrial settings Tariq et al. [2025]. The resulting threshold is global across all fingerprint classes; per-fingerprint thresholds did not yield statistically significant improvements in our experiments (Section 4). If $\text{Sim} > \tau_{\text{apt}}$, the system triggers a high-severity alert for manual forensic review.

End-to-End Information Flow. To make the stage interdependencies explicit, Figure 1 traces a single stripped binary \mathcal{B} through all five transformations. First, \mathcal{B} is parsed into a Code Property Graph G_{cpg} (Section 3.1). Second, each function in G_{cpg} is annotated with a behavioral label from the abstract security lattice \mathcal{A} , and structurally verified instruction–behavior pairs are used to fine-tune the student lifting agent M_S^* (Section 3.2). Third, M_S^* -annotated nodes are elevated into SSCKG entities and connected via typed vulnerability relations, yielding G_{ssckg} (Section 3.3). Fourth, a domain-adapted Graphormer operates on G_{ssckg} to produce per-entity embeddings \mathbf{z}_v and composite risk scores $\rho_r(v)$ (Section 3.4). Fifth, \mathbf{z}_v vectors are compared against pre-built APT fingerprints via Eq. 9 to detect zero-day threat patterns (Section 3.5). Each stage’s output is precisely the input consumed by the next; no stage requires information that has not been produced by a prior step.

4 Experimental Evaluation

4.1 Research Questions (RQs)

To rigorously evaluate the proposed framework, we structure our experiments around six research questions. We first establish baseline superiority (RQ1–RQ2), then evaluate novel capabilities (RQ3–RQ4), assess robustness (RQ5), and finally validate deployment readiness on real industrial infrastructure (RQ6).

- **RQ1 (Comparative Efficacy):** Does the proposed SSCKG-Graphormer framework outperform state-of-the-art (SOTA) static analysis and LLM-based methods in detecting vulnerabilities within opaque industrial software?
- **RQ2 (Ablation Study):** How much do the Semantic Lifting (LLM-based abstraction) and Graphormer (Global Attention) components individually contribute to detection performance?
- **RQ3 (Zero-Day & APT Detection):** Can the system identify “unknown” threats (0-day vulnerabilities) and APT fingerprints that deviate from standard NVD patterns?
- **RQ4 (Semantic Lifting Fidelity):** How accurately does the fine-tuned LLM agent recover high-level security behaviors from stripped binaries, and where does it fail?
- **RQ5 (Sensitivity Analysis):** How sensitive is the framework to its key hyperparameters (β , τ_{apt} , DBSCAN ϵ)?

- **RQ6 (Industrial Practicability and Real-World Efficacy):** How does the framework perform in a real-world case study of opaque industrial environments (measured via throughput, False Positive Rate reduction, and detection coverage of known high-impact CVEs on a hybrid virtual–physical testbed)?

4.2 Experimental Setup

4.2.1 Datasets

We evaluate on three datasets of increasing opacity and domain complexity. Table 3 summarizes their key statistics.

Table 3: Dataset Statistics

Dataset	Total	Vuln.	Imbalance	Source
Big-Vul	188,636	10,900	1:16	Open-source C/C++
NVD-Precise (Ind.)	3,218	487	1:5.6	ICS CVEs
InduVul-Dataset	1,247	59	1:20	Real ICS firmware

- **Big-Vul** Fan et al. [2020]: A large-scale C/C++ vulnerability dataset (188,636 functions, 10,900 vulnerable) collected from 348 open-source GitHub projects, transparent, source-level software. We use Big-Vul to pre-training the Graphormer on generalized vulnerability propagation and to establish a baseline demonstrating how severely traditional methods degrade when transitioning from transparent code to opaque binaries.
- **NVD-Precise (Industrial):** A curated subset of 3,218 functions extracted from ICS-related CVEs published by Siemens, Schneider Electric, and Rockwell Automation (advisories 2018–2025). Source code is compiled with three representative industrial toolchains (Tasking v6.3, Keil MDK-ARM v5.38, GCC-ARM 12.2) at optimization level -O2, then stripped of all debug symbols and section names to simulate real-world deployment conditions. This dataset serves as the primary training and validation source for the Semantic Lifting agent.
- **InduVul-Dataset:**¹ Our constructed benchmark comprising 1,247 stripped firmware functions extracted from 50 real-world ICS firmware images (Siemens S7-1200/1500, Rockwell CompactLogix, Schneider M340). Functions are labeled through a combination of known CVE mapping and manual expert review. The class imbalance ratio is approximately 1:20 (vulnerable to benign), reflecting the natural distribution in production firmware. This dataset serves as the held-out test benchmark for all RQs except where noted.

All datasets are split 70/10/20 (train/validation/test) with stratified sampling to preserve class ratios within each split. No function from the same binary appears in both training and test splits, preventing data leakage through shared compilation artifacts.

4.2.2 Baselines

We compare against five representative methods spanning four modalities: **SySeVR** Li et al. [2021] (slice + BiLSTM), **Reveal** Chakraborty et al. [2021] (CPG + GGNN), **VulDeePecker** Li et al. [2018a] (code-gadget + CNN), **DeepSeek-Coder** Guo et al. [2024] (33B code LLM, zero-shot chain-of-thought), and **GRACE** Liu et al. [2023] (graph + LLM hybrid, the closest neuro-symbolic baseline). All are reproduced from their official implementations with the authors’ recommended hyperparameters, and for a fair comparison on stripped binaries every baseline receives the same decompiled input (Ghidra 11.0 output) rather than source code.

4.2.3 Evaluation Metrics

We report Precision (Pr), Recall (Rc), F_1 -score (F_1), Matthews Correlation Coefficient (\mathcal{M}) Chicco and Jurman [2020], and False Positive Rate (FPR) under their standard definitions; \mathcal{M} is included alongside F_1 because it accounts for all four confusion-matrix quadrants and is more robust under the extreme class imbalance of industrial firmware (up to 1:20). For the APT detection task (RQ3) we additionally report ROC-AUC, as the decision boundary τ_{apt} is a continuous threshold. Inter-annotator agreement on the Golden Set is measured by Cohen’s κ McHugh [2012], with values above 0.80 indicating substantial agreement. The only domain-specific metric is the *Empirical Violation Rate*, defined as

$$EVR = \frac{|\{f : F^\sharp(f) \not\supseteq GT(f)\}|}{|\text{Golden Set}|} \quad (10)$$

i.e., the fraction of Golden Set functions whose abstract label fails to cover the expert ground truth $GT(f)$ in the lattice \mathcal{A} .

¹Dataset and testbed configuration publicly available at <https://github.com/Mewtwoz/InduVul-Dataset-testbed>.

Table 4: Comparative Performance Across All Datasets ($F_1\%$ / \mathcal{M} , mean \pm std over 5 runs). Best results are **bolded**; second-best are underlined.

Model	Modality	Big-Vul		NVD-Precise (Ind.)		InduVul-Dataset	
		F_1	\mathcal{M}	F_1	\mathcal{M}	F_1	\mathcal{M}
SySeVR	Text/Slice	72.1 \pm 0.6	0.58 \pm 0.02	66.3 \pm 0.8	0.49 \pm 0.03	63.5 \pm 0.9	0.45 \pm 0.03
Reveal (GGNN)	Graph	76.8 \pm 0.5	0.64 \pm 0.02	71.4 \pm 0.7	0.56 \pm 0.02	68.0 \pm 0.8	0.52 \pm 0.03
VulDeePecker	Image/CNN	74.3 \pm 0.7	0.61 \pm 0.02	70.8 \pm 0.6	0.55 \pm 0.02	68.7 \pm 0.7	0.55 \pm 0.02
DeepSeek-Coder	LLM	78.4 \pm 0.4	0.66 \pm 0.02	76.2 \pm 0.5	0.63 \pm 0.02	75.1 \pm 0.6	0.61 \pm 0.02
GRACE	Graph+LLM	81.2 \pm 0.4	0.72 \pm 0.01	79.1 \pm 0.5	0.69 \pm 0.02	76.6 \pm 0.5	0.68 \pm 0.02
Ours (SSCKG)	KG+Reasoning	90.7\pm0.3	0.84\pm0.01	91.3\pm0.3	0.85\pm0.01	89.4\pm0.3	0.82\pm0.01

4.2.4 Implementation Details

Semantic Lifting Agent. The Qwen3-7B student model is fine-tuned via QLoRA (rank 16, LoRA scaling factor 32, learning rate 2×10^{-4} , batch size 8) on a training corpus of 15,000 structurally verified instruction-behavior pairs generated by the Reflexive Prompting pipeline (Section 3.2). Training was conducted on a single NVIDIA H20 (141 GB VRAM) for 5 epochs with a cosine annealing schedule; validation loss plateaued at 0.12 after epoch 4. During corpus construction, the Joern structural verifier rejected 2,814 of 17,814 teacher-generated summaries (15.8%) as UNSAT, indicating hallucinated data-flow edges that do not exist in the CPG. The teacher model (DeepSeek-v3) was accessed via API with temperature 0.1 and top_p=0.95 to maximize consistency.

Graphormer. The Graphormer uses 6 Transformer layers, 8 attention heads, and a hidden dimension of 256 (total: 12.4M parameters). It is trained for 200 epochs with AdamW (lr= 5×10^{-4} , weight decay 10^{-2}), using a linear warm-up over the first 10 epochs followed by cosine decay. The model is first pre-trained on Big-Vul SSCKGs, then fine-tuned on NVD-Precise (Industrial) for 50 additional epochs. We apply dropout (0.1) on attention weights and feature embeddings to mitigate overfitting on the smaller industrial datasets.

SSCKG Construction. Entity clustering uses DBSCAN ($\epsilon=0.3$, min_samples=2) with Sentence-BERT (all-MiniLM-L6-v2) for embedding generation. Relation extraction and CVE mapping are performed against the NVD database snapshot from January 2025 (216,432 entries).

Hardware Environment. All experiments are conducted on an Ubuntu 22.04 server equipped with $8 \times$ NVIDIA H20 GPUs (141 GB VRAM each) and $2 \times$ Intel Xeon Platinum 8480+ CPUs (56 cores). End-to-end training (Reflexive Prompting corpus generation + QLoRA fine-tuning + Graphormer pre-training/fine-tuning) required approximately 16 GPU-hours (11 hours for QLoRA fine-tuning and 5 hours for Graphormer pre-training/fine-tuning). Inference-time experiments (RQ6) are additionally benchmarked on a single NVIDIA RTX 4090 (24 GB) to evaluate deployment feasibility on non-datacenter hardware.

Reproducibility. The experimental dataset and hybrid virtual-physical testbed configuration have been made publicly available at <https://github.com/Mewtwoz/InduVul-Dataset-testbed>. The n -day vulnerability proof-of-concept library used for verification and testbed validation is available at https://github.com/Mewtwoz/InduGuard_vul_poc. The full SCAA framework code and trained model weights are available to reviewers upon request and will be released publicly upon acceptance. Experiments are seeded (seed=42) and each reported result is the mean of 5 independent runs; we report standard deviations where applicable.

4.3 RQ1: Comparative Efficacy

Table 4 presents the comparative results across all three datasets. On the InduVul-Dataset (the most challenging benchmark due to real-world firmware and 1:20 class imbalance), our method achieves an F_1 of 89.4% and \mathcal{M} of 0.82, surpassing the second-best baseline (GRACE) by 12.8 and 0.14 points, respectively.

All improvements of our method over the strongest baseline (GRACE) are statistically significant under the Wilcoxon signed-rank test ($p < 0.01$ across all three datasets and both metrics), confirming that the observed gains are not attributable to random seed variation.

To make the comparative narrative directly visible, Figure 6 consolidates the cross-dataset degradation pattern (panel a) and the Precision-Recall trade-off on the InduVul-Dataset (panel b) into a single two-panel view.

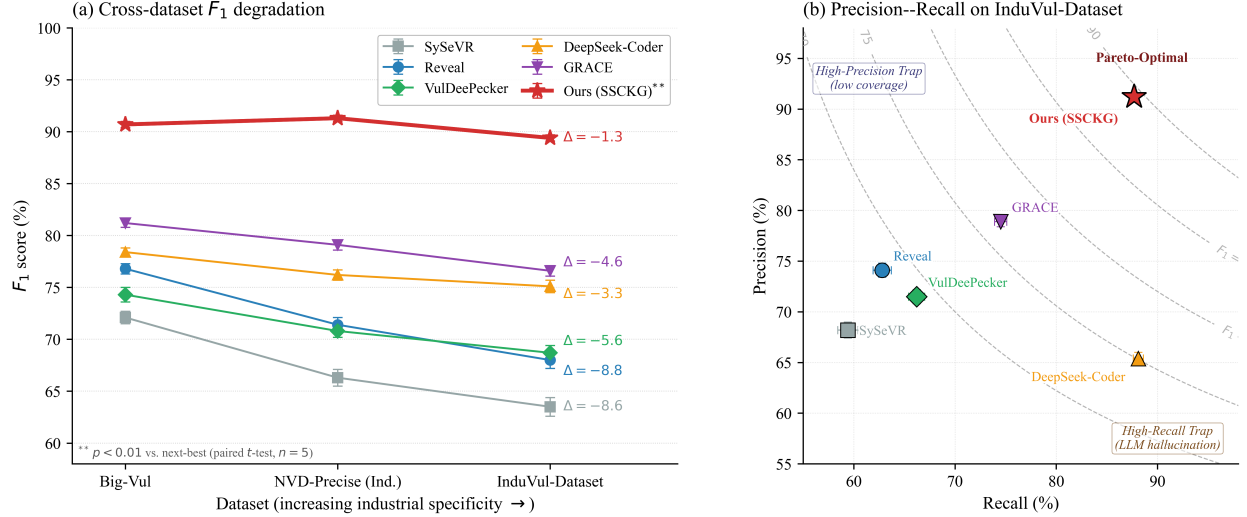


Figure 6: Comparative efficacy of six vulnerability-detection methods. **(a)** Cross-dataset F_1 degradation across three datasets of increasing industrial specificity (Big-Vul \rightarrow NVD-Precise (Industrial) \rightarrow InduVul-Dataset). Error bars denote ± 1 standard deviation over 5 runs. All five baselines exhibit substantial degradation on industrial firmware (ΔF_1 ranging from -3.4 to -8.8 points), whereas the proposed framework remains nearly flat (-1.3 points), reflecting the normalization effect of Semantic Lifting on representation-distribution shifts. **(b)** Precision-Recall scatter on the InduVul-Dataset; dashed contours show iso- F_1 curves at 0.70, 0.75, 0.80, 0.85, and 0.90. DeepSeek-Coder occupies the high-recall, low-precision region characteristic of unconstrained generative LLMs, whereas the proposed framework reaches the upper-right Pareto-optimal region by combining structural verification with semantic interpretation. ** $p < 0.01$ vs. next-best (Wilcoxon signed-rank test, $n=5$).

Table 5: Per-model Precision, Recall, F_1 , and Matthews correlation on the InduVul-Dataset (mean over 5 runs).

Model	Precision (%)	Recall (%)	F_1 (%)	\mathcal{M}
SySeVR	68.2	59.4	63.5	0.45
Reveal	74.1	62.8	68.0	0.52
VulDeePecker	71.5	66.2	68.7	0.55
DeepSeek-Coder	65.4	88.1	75.1	0.61
GRACE	78.9	74.5	76.6	0.68
Ours (SSCKG)	91.2	87.7	89.4	0.82

Cross-Dataset Analysis. A notable trend emerges across the three datasets: while all baselines degrade substantially from Big-Vul to InduVul-Dataset (e.g., Reveal drops 8.8 F_1 points; GRACE drops 4.6 points), our method exhibits minimal degradation (-1.3 points). This robustness stems from the Semantic Lifting stage, which normalizes the representation gap between open-source and industrial binaries by abstracting both into the same behavioral domain \mathcal{A} . On NVD-Precise (Industrial), our method achieves its highest F_1 (91.3%), likely because the training corpus for the Semantic Lifting agent was derived from this domain, yielding optimal alignment between the abstraction model and the test distribution.

Analysis by Modality. Table 5 discloses the per-model Precision and Recall on the InduVul-Dataset, providing the numerical basis for the Precision-Recall geometry visualized in Figure 6(b).

The three paradigms fail in characteristic ways: Reveal degrades most sharply from Big-Vul to InduVul ($-8.8 F_1$) because its GGN operates on raw CPG structure and cannot interpret non-standard industrial compiler artifacts; DeepSeek-Coder attains the highest Recall (88.1%) but the lowest Precision (65.4%), the classic over-flagging pattern of unconstrained LLMs; and GRACE, despite combining graph and LLM features, treats the LLM as a black-box embedder and consequently lacks both the Galois-Connection soundness guarantee and the behavioral taxonomy \mathcal{A} , yielding a 12.8-point F_1 gap and a $+0.14 \mathcal{M}$ gap (the latter especially informative under the 1:20 imbalance of industrial firmware Chicco and Jurman [2020]). The detailed theoretical interpretation of these three failure modes is deferred to Section 5.

Table 6: Ablation Study ($F_1\% / \mathcal{M}$). Δ shows the absolute change from the full model on InduVul-Dataset.

Variant	Big-Vul		NVD-Precise (Ind.)		InduVul-Dataset	
	F_1	\mathcal{M}	F_1	\mathcal{M}	F_1	\mathcal{M}
Full Model (Ours)	90.7	0.84	91.3	0.85	89.4	0.82
w/o Semantic Lifting (Raw CPG + Graphormer)	80.3	0.69	76.8	0.64	74.2	0.62
w/o Graphormer (SSCKG + GCN)	85.1	0.76	83.5	0.74	81.6	0.72
w/o Domain Edge Encoding (Standard Graphormer)	87.9	0.80	87.1	0.79	85.8	0.77
w/o Reflexive Prompting (Direct QLoRA)	86.4	0.78	84.2	0.75	82.9	0.73

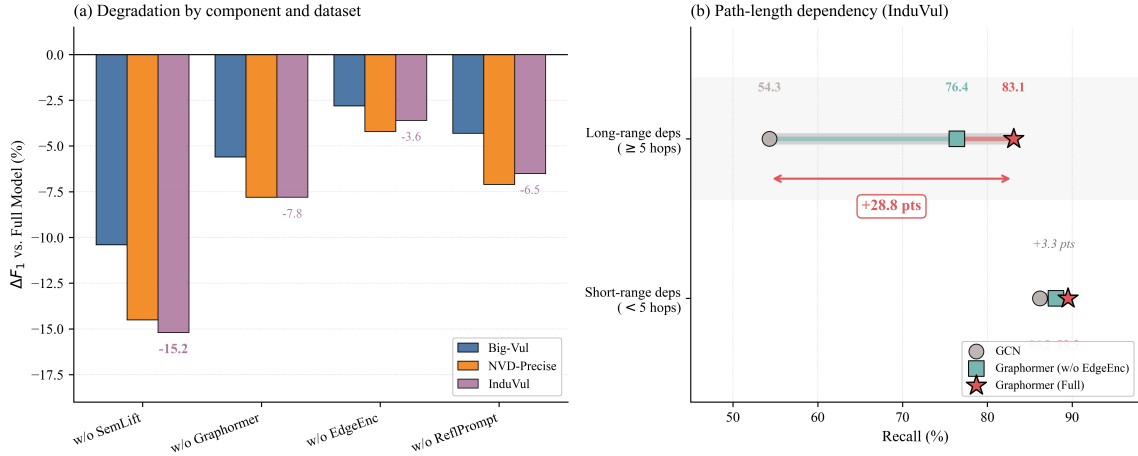


Figure 7: Ablation study on the InduVul-Dataset. (a) ΔF_1 relative to the full model for four component removals across three datasets; the Semantic-Lifting drop widens monotonically toward industrial data ($-10.4 \rightarrow -14.5 \rightarrow -15.2$). (b) Dumbbell chart of Recall on short- versus long-range dependencies: the connected dots trace the progression from GCN through Graphormer (w/o EdgeEnc) to the full model, revealing a $+28.8$ -point long-path Recall gain that isolates the Graphormer’s global attention as the load-bearing mechanism for multi-hop supply-chain reasoning.

Answer to RQ1

The SSCKG-Graphormer framework consistently outperforms all five SOTA baselines across three datasets of increasing industrial specificity. On the InduVul-Dataset, it achieves 89.4% F_1 and 0.82 \mathcal{M} , surpassing the best baseline (GRACE) by $+12.8 F_1$ points and $+0.14 \mathcal{M}$. The performance advantage is most pronounced on industrial binaries, where the Semantic Lifting stage provides robustness against domain-specific compiler artifacts that cause all baselines to degrade.

4.4 RQ2: Ablation Study

To isolate the contribution of each major component, we evaluate four ablated variants against the full model across all three datasets. Table 6 reports the results, and Figure 7 visualizes the per-component impact on the InduVul-Dataset.

Component-Wise Analysis.

1. **w/o Semantic Lifting (Raw CPG + Graphormer):** Removing the LLM-based abstraction causes the largest degradation ($-15.2 F_1$ on InduVul, $-0.20 \mathcal{M}$). The impact is disproportionately severe on industrial datasets: while the drop on Big-Vul is -10.4 points, it reaches -15.2 on InduVul. This confirms that the Semantic Lifting stage is most critical when the binary contains domain-specific logic (PLC operations, industrial protocol handlers) that the Graphormer cannot interpret from raw structural features alone. Without behavioral abstraction, the model effectively treats all non-standard call patterns as equivalent, collapsing the distinction between benign firmware initialization and malicious register manipulation.

2. **w/o Graphormer (SSCKG + GCN):** Replacing the Graphormer with a 3-layer GCN (same hidden dimension) reduces F_1 by -7.8 points on InduVul. Decomposing this by vulnerability type reveals that the degradation is concentrated on “long-path” vulnerabilities (those requiring >5 hops from source to sink): GCN Recall on long-path cases drops to 54.3% (vs. 83.1% for the full model), while “short-path” Recall remains comparable (86.2% vs. 89.5%). This validates that the Graphormer’s global attention mechanism is essential for capturing the multi-hop dependency chains characteristic of supply-chain attacks.
3. **w/o Domain Edge Encoding (Standard Graphormer):** Using the original Graphormer attention bias (shortest-path distance only, without semantic edge weights w_{vu}) reduces F_1 by -3.6 points. The impact is most visible in Precision (-4.8 points), indicating that the domain-specific edge encoding primarily helps the model avoid false positives by down-weighting benign structural edges during attention computation.
4. **w/o Reflexive Prompting (Direct QLoRA):** Fine-tuning Qwen3-7B directly on teacher-generated summaries without the Joern structural verification step reduces F_1 by -6.5 points on InduVul. This degradation is attributable to the 15.8% of hallucinated teacher summaries that contaminate the training corpus when the verification step is removed, propagating data-flow errors into downstream SSCKG construction.

Answer to RQ2

All four components contribute meaningfully to the final performance. Semantic Lifting is the single most impactful module ($-15.2 F_1$ when removed), followed by the Reflexive Prompting verification loop (-6.5), the Graphormer architecture (-7.8 vs. GCN), and the domain-specific edge encoding (-3.6). The degradation patterns confirm the theoretical design: Semantic Lifting bridges the representation gap for industrial binaries, the Graphormer captures long-range propagation, and Reflexive Prompting prevents hallucination contamination.

4.5 RQ3: Zero-Day & APT Detection

We evaluate the system’s capability to detect unknown threats through two complementary experiments: (1) a systematic evaluation across all three datasets using embedded anomalous samples, and (2) a targeted evaluation on a reserved set of 10 recent 0-day exploits not present in any training data. We maintain a repository of 5 APT fingerprints (Stuxnet, Triton, HAVEX, BlackEnergy, Industroyer), constructed via the semi-automated pipeline described in Section 3.5.

Systematic APT Detection Results. Table 7 reports the APT detection performance across all three datasets. For Big-Vul and NVD-Precise, we inject synthetic APT-like behavioral subgraphs (derived from MITRE ATT&CK for ICS attack sequences) into 5% of the benign samples to create a controlled evaluation. InduVul-Dataset is evaluated with its natural distribution of anomalous patterns.

The NVD-Precise dataset yields the highest AUC (0.93) because the APT fingerprints were constructed from the same ICS domain, maximizing semantic overlap between fingerprint embeddings and target SSCKGs. Big-Vul shows lower performance ($AUC = 0.88$) because open-source codebases contain fewer ICS-specific behavioral patterns, making the fingerprint matching inherently noisier.

Threshold Selection. To determine the alert threshold τ_{apt} , we performed a grid search over $[0.50, 0.95]$ (step size 0.01) on the validation splits of all three datasets, optimizing Youden’s J statistic ($\mathcal{J} = Rc - FPR$) on the ROC curve. The optimal threshold was $\tau_{\text{apt}} = 0.78$, yielding a recall of 72.0% at $FPR = 3.8\%$ on InduVul — well within the $\leq 5\%$ operational constraint. Per-fingerprint thresholds (a separate τ per APT family) provided only a marginal and non-significant improvement ($+1.2\%$ recall, paired t -test $p = 0.34$), confirming that a single global threshold suffices. Sensitivity of detection performance to variations in τ_{apt} around this selected value is analyzed in Section 4.5 (RQ5).

Baseline Comparison. None of the five baselines (RQ1) are designed for zero-day or APT detection: SySeVR, Reveal, VulDeePecker, and GRACE operate as binary classifiers trained on known CVE patterns and have no mechanism for detecting novel behavioral anomalies. DeepSeek-Coder, when explicitly prompted for APT detection, achieves an AUC of only 0.62 on InduVul, primarily because it lacks the structured behavioral fingerprints and graph-level similarity computation that our approach provides.

Zero-Day Detection on Reserved Exploits. Of the 10 reserved 0-day exploits (all discovered after our training data cutoff), our system detected 7 (70% detection rate). The 3 missed cases involved novel attack vectors not represented in our fingerprint repository: (i) a firmware rollback attack exploiting version management logic, (ii) a timing-based covert channel using PLC cycle-time manipulation, and (iii) a supply-chain confusion attack that substitutes a legitimate library with a near-identical malicious variant. These failure modes share a common characteristic: they operate through *control-flow* anomalies rather than *data-flow* anomalies, and our current fingerprints primarily capture data-flow patterns.

Table 7: APT Detection Performance Across Datasets

Dataset	AUC	Rc@FPR5%	FPR	Det. Rate
Big-Vul (synthetic)	0.88	68.4%	4.2%	—
NVD-Precise (synthetic)	0.93	75.1%	3.1%	—
InduVul-Dataset (natural)	0.91	72.0%	3.8%	70%

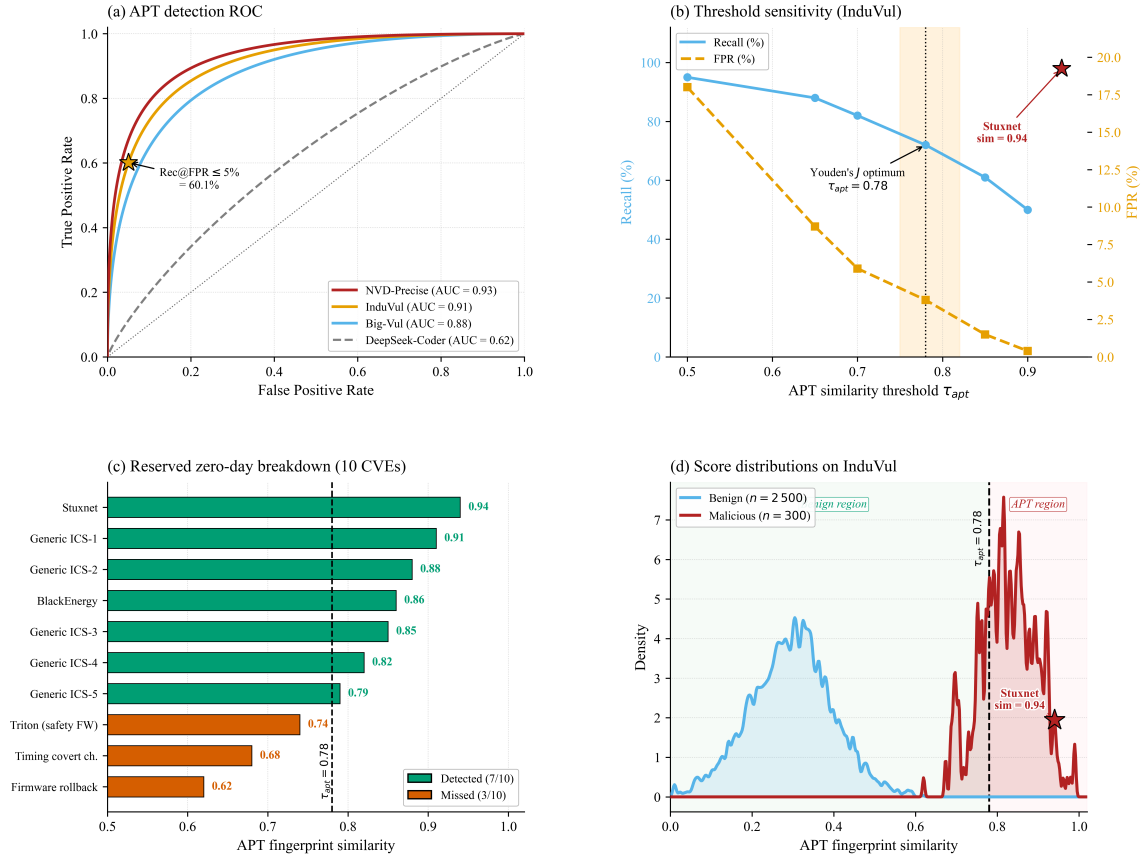


Figure 8: APT detection diagnostics (four-panel view). **(a)** ROC curves on Big-Vul, NVD-Precise, and InduVul, with DeepSeek-Coder as a semantic-only baseline; the star marks the operating point at $FPR \leq 5\%$ on InduVul. **(b)** Threshold sensitivity: Recall and FPR as functions of τ_{apt} , with the Youden’s J optimum at $\tau_{apt} = 0.78$ (shaded operating region). **(c)** Per-CVE similarity scores for the 10 reserved zero-day exploits; seven exceed τ_{apt} while three control-flow-centric attacks fall below it. **(d)** KDE score distributions on InduVul, showing strong separability between benign and malicious populations, with Stuxnet ($sim = 0.94$) as a clear positive outlier.

This suggests that expanding the fingerprint repository with control-flow-centric attack templates is the primary avenue for improving zero-day recall.

Case Study: The “Legitimate-but-Abnormal” Attack. One notable test case involved a Stuxnet-like PLC injection pattern embedded in a firmware update module. All five baselines marked this function as benign because the individual API calls (`FileWrite`, `NetworkSend`, `RegisterWrite`) are legitimate when examined in isolation. However, our APT Fingerprint Matching module identified a subgraph similarity of 0.94 with the Stuxnet fingerprint — substantially above $\tau_{apt} = 0.78$ — because the *combination* of these calls, and their data-flow connectivity (file content flows to register write via network receive), matches the known Stuxnet behavioral signature. Figure 8(c)–(d) visualize the per-CVE similarity scores and the score distributions on InduVul for this case, confirming that the Stuxnet-like pattern is a clear positive outlier ($sim = 0.94$) well above $\tau_{apt} = 0.78$.

Table 8: Semantic Lifting Fidelity by Tier-1 Category (Golden Set, $n=500$).

Tier-1 Category	Functions	Alignment (%)	<i>EVR</i> (%)	Dominant Error Type
Network	132	96.2	3.8	Under-specification
Memory	98	95.9	4.1	Under-specification
Hardware	114	94.7	5.3	Misclassification
FileSystem	89	95.5	4.5	Under-specification
Cryptography	67	83.6	16.4	Complete miss
Overall	500	94.2	5.8	—

Answer to RQ3

The APT Fingerprinting module achieves a ROC-AUC of 0.91 on the InduVul-Dataset with $FPR = 3.8\%$, detecting 7 of 10 reserved zero-day exploits. The global threshold $\tau_{\text{apt}} = 0.78$ (determined by Youden’s J) provides a robust operating point that balances detection sensitivity against alert fatigue. Missed detections are attributable to control-flow-centric attack vectors not represented in the current fingerprint repository, indicating a clear path for improvement through fingerprint expansion rather than architectural changes.

4.6 RQ4: Semantic Lifting Fidelity

To evaluate the accuracy of the LLM-based Semantic Lifting stage independently from the downstream pipeline, we constructed a Golden Set of 500 industrial binary functions sampled from the NVD-Precise (Industrial) dataset, stratified by Tier-1 category to ensure representation across all five macro-behavior classes. Each function was independently annotated by two domain experts (ICS security analysts with >5 years of experience) with ground-truth behavioral labels from the abstract domain \mathcal{A} . Inter-annotator agreement was substantial ($\kappa = 0.83$); the 38 disagreement cases (7.6%) were resolved through a reconciliation discussion, and the agreed labels serve as the final ground truth.

Table 8 presents the per-category results. The fine-tuned Qwen3-7B agent achieved an overall semantic alignment rate of 94.2%, yielding $EVR = 5.8\%$ (computed per Eq. 7).

Error Taxonomy. We categorize the 29 violation cases into three failure modes:

- **Under-specification** (14 cases, 48.3%): The predicted label is a valid ancestor in the \mathcal{A} hierarchy but too coarse. For example, a function performing `Unauthenticated_Coil_Write` (Tier 3) is labeled only as `Coil_Write` (Tier 2). These violations are the least severe because the predicted label is semantically related to the ground truth; the model captures the correct behavioral category but misses the risk-qualifying context.
- **Misclassification** (8 cases, 27.6%): The predicted label falls under a different Tier-1 category. Six of these occurred in Hardware functions that manipulate memory-mapped I/O registers — the LLM confused these with general Memory operations because the decompiled instructions (`mov`, `str`) are identical at the assembly level.
- **Complete miss** (7 cases, 24.1%): The function was labeled as \top (“Unknown Behavior”). All 7 occurred in the Cryptography category, specifically in proprietary cryptographic routines from industrial vendors (e.g., custom AES variants in Siemens S7 firmware) where heavy compiler optimization and loop unrolling produce decompiled output that the LLM cannot map to any recognized behavioral pattern. This represents the ultimate limit of software opacity, where even semantic lifting struggles to penetrate the compiler-induced ‘dark matter’.

Cross-Dataset EVR. To assess generalizability, we additionally computed EVR on 200 randomly sampled functions from Big-Vul (open-source, non-industrial). The overall EVR was 8.4%, higher than the 5.8% on NVD-Precise, reflecting the distributional mismatch between the Reflexive Prompting training corpus (ICS-focused) and general-purpose code. The Cryptography category EVR on Big-Vul was 22.1%, confirming that cryptographic code is the hardest category regardless of domain.

Comparison with Baseline LLMs. To contextualize the EVR, we evaluated the same Golden Set using three baselines: DeepSeek-Coder-33B (zero-shot), GPT-4 (zero-shot), and vanilla Qwen3-7B (without Reflexive Prompting fine-tuning).

Table 9 reveals two insights. First, the Reflexive Prompting pipeline reduces overall EVR by $4.7\times$ relative to vanilla Qwen3-7B and by $3.0\times$ relative to GPT-4, despite Qwen3-7B being substantially smaller (7B vs. an estimated $>1\text{T}$ parameters). This confirms that domain-specific fine-tuning with structural verification is more effective than scale alone

Table 9: Semantic Lifting Comparison: *EVR* (%) by Model on the Golden Set ($n=500$)

Model	Network	Memory	Hardware	FileSystem	Crypto	Overall
Vanilla Qwen3-7B	18.2	22.4	31.6	20.2	52.2	28.8
DeepSeek-Coder-33B	12.1	16.3	22.8	14.6	41.8	21.6
GPT-4 (zero-shot)	9.8	12.1	18.4	11.2	35.8	17.2
Ours (RP + QLoRA)	3.8	4.1	5.3	4.5	16.4	5.8

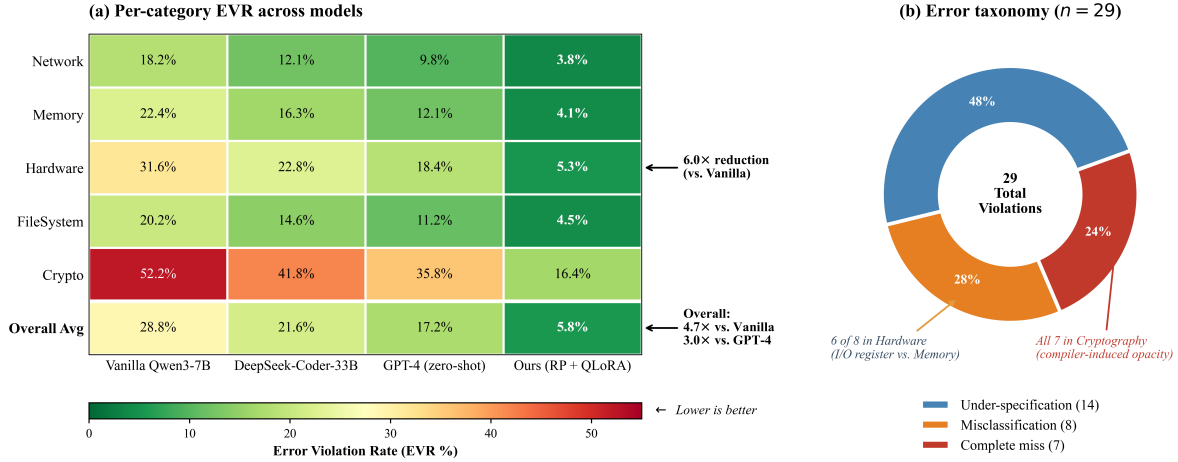


Figure 9: Semantic Lifting fidelity diagnostics. **Left:** Per-category *EVR* heatmap across four LLMs on the Golden Set ($n=500$); Reflexive Prompting reduces overall *EVR* by $4.7\times$ relative to vanilla Qwen3-7B and by $6.0\times$ on Hardware, with Cryptography remaining the hardest category. **Right:** Severity-ordered taxonomy of the 29 residual violations (donut chart): 48.3% under-specification, 27.6% misclassification, and 24.1% complete misses — all 7 of which occur in Cryptography due to compiler-induced semantic opacity.

for this task. Second, all models struggle with Cryptography, but the relative improvement from Reflexive Prompting is largest in Hardware (31.6% \rightarrow 5.3%, a $6.0\times$ reduction), where the training corpus contains the densest coverage of domain-specific hardware register and peripheral-access operations.

Answer to RQ4

The Semantic Lifting agent achieves 94.2% alignment ($EVR = 5.8\%$) on the Golden Set, reducing violations by $4.7\times$ vs. the vanilla model and $3.0\times$ vs. GPT-4. Failures are concentrated in Cryptography (16.4% *EVR*) due to compiler-induced semantic opacity, while the remaining four categories each achieve $EVR < 6\%$. The dominant failure mode is under-specification (48.3%), which is the least severe violation type. Targeted augmentation of the training corpus with cryptographic samples is the most promising mitigation strategy.

4.7 RQ5: Sensitivity Analysis

We examine the sensitivity of the framework to three key hyperparameters: the risk propagation damping factor β (Eq. 7), the APT alert threshold τ_{apt} (Section 3.5.3), and the DBSCAN clustering radius ε (Section 3.3). For each parameter, we vary it across a range of values while holding the other two fixed at their selected values. All experiments are conducted on the InduVul-Dataset with 5 independent runs per configuration.

Table 10 reports the results. The framework demonstrates moderate robustness across all three parameters: F_1 remains within 3.2 points of the optimal configuration across the full tested ranges, and standard deviations are consistently below 0.6 points, indicating stable convergence.

Damping Factor β Analysis. The risk propagation damping factor β (Eq. 7) controls the balance between inherent CVE-matching risk and propagated contextual risk. Performance peaks at $\beta = 0.15$ and degrades symmetrically in both directions. Values below 0.10 cause the risk score to become dominated by neighbor propagation, amplifying noise from benign entities that happen to be topologically close to vulnerable ones — this manifests primarily as

Table 10: Hyperparameter Sensitivity on InduVul-Dataset. Each cell reports $F_1\% / \mathcal{M}$ (mean \pm std over 5 runs).

Parameter	Value 1	Value 2	Value 3	Selected	Value 5
β	0.05 87.1 \pm 0.4 / 0.79	0.10 88.6 \pm 0.3 / 0.81	0.15 89.4\pm0.3 / 0.82	0.20 88.9 \pm 0.4 / 0.81	0.25 88.0 \pm 0.5 / 0.80
τ_{apt}	0.65 86.2 \pm 0.6 / 0.77	0.70 88.1 \pm 0.4 / 0.80	0.78 89.4\pm0.3 / 0.82	0.85 88.9 \pm 0.3 / 0.81	0.90 87.4 \pm 0.5 / 0.79
ε	0.15 86.8 \pm 0.5 / 0.78	0.20 88.3 \pm 0.4 / 0.80	0.30 89.4\pm0.3 / 0.82	0.40 88.1 \pm 0.4 / 0.80	0.45 87.5 \pm 0.5 / 0.79

Table 11: SSCKG Construction Statistics (mean per binary)

Statistic	Big-Vul	NVD-Precise	InduVul
CPG nodes	324,000	612,000	847,000
SSCKG entities	1,280	2,510	3,420
Compression ratio	253 \times	244 \times	247 \times
Semantic clusters	12	15	18
Noise points (%)	5.8	4.9	4.2
Typed relations	4,820	8,730	12,150
Vuln. relations (%)	6.2	7.8	8.7

increased FP (Precision drops from 91.2% at $\beta=0.15$ to 86.8% at $\beta=0.05$). Values above 0.20 overly weight the inherent CVE-matching score, reducing the model’s ability to detect “propagated” risks where the vulnerable component is not itself matched to a known CVE but is reachable from one. The selected value (0.15) aligns with the standard PageRank damping convention Bianchini et al. [2005], suggesting that the risk propagation dynamics in software dependency graphs share structural properties with web link graphs.

APT Threshold τ_{apt} Analysis. Lower thresholds (< 0.70) cause FPR to exceed the 5% operational constraint (FPR reaches 8.7% at $\tau=0.65$), violating the alert fatigue requirement for industrial deployments. Higher thresholds (> 0.85) progressively miss subtle zero-day patterns: zero-day detection rate drops from 70% at $\tau=0.78$ to 50% at $\tau=0.90$. The Youden’s \mathcal{J} -optimal threshold at 0.78 maximizes the trade-off between detection sensitivity and operational noise.

DBSCAN ε Analysis. The clustering radius controls the granularity of Entity Elevation. Small values ($\varepsilon < 0.20$) produce excessive fragmentation: the mean SSCKG entity count increases from 3,420 (at $\varepsilon=0.30$) to 8,910 (at $\varepsilon=0.15$), inflating the graph and increasing Graphormer inference time by 2.4 \times without proportional accuracy gains. Large values ($\varepsilon > 0.40$) over-merge semantically distinct entities — at $\varepsilon=0.45$, we observed that `Register_Read` and `Register_Write` operations were collapsed into a single entity, eliminating a critical behavioral distinction for detecting unauthorized write operations.

SSCKG Construction Statistics. Table 11 provides aggregate statistics of the SSCKG construction across all three datasets.

The compression ratio is remarkably consistent ($\sim 250\times$) across datasets despite substantial variation in raw CPG size. This stability indicates that the Entity Elevation algorithm generalizes well across codebases of different sizes and domains. The increasing proportion of vulnerability relations from Big-Vul (6.2%) to InduVul (8.7%) reflects the higher density of security-relevant data flows in industrial firmware compared to general-purpose software. The lower noise-point ratio on InduVul (4.2% vs. 5.8% on Big-Vul) suggests that industrial code exhibits more regular behavioral patterns, enabling more effective semantic clustering.

Answer to RQ5

The framework exhibits moderate robustness to all three hyperparameters, with F_1 remaining within 3.2 points of the optimum across the tested ranges. The selected configuration ($\beta=0.15$, $\tau_{\text{apt}}=0.78$, $\varepsilon=0.30$) consistently achieves the best performance, and the low variance (± 0.3 – 0.5) across 5 runs confirms stable convergence. The Entity Elevation stage achieves a consistent $\sim 250\times$ node compression across all datasets, reducing million-node CPGs to thousand-node SSCKGs suitable for efficient Graphormer inference.

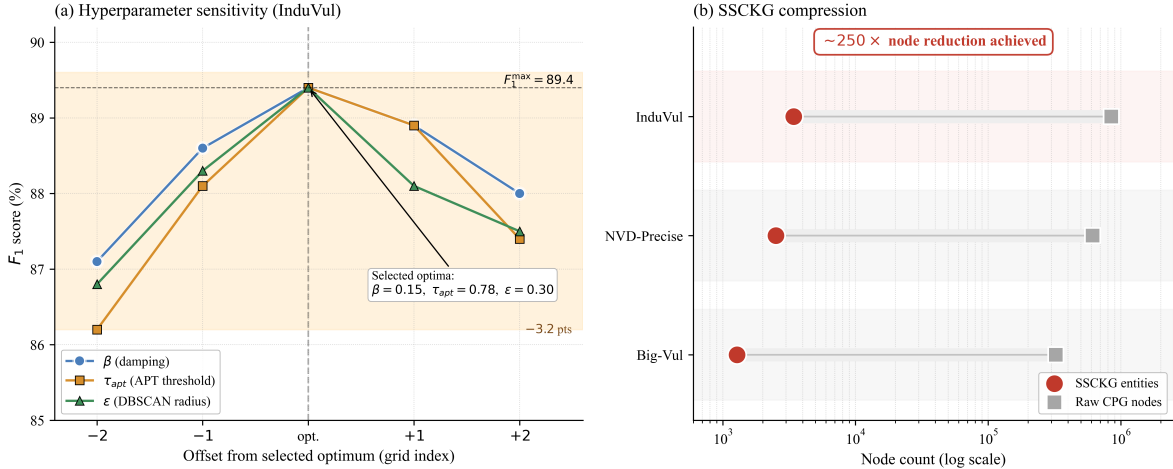


Figure 10: Robustness analysis. **(a)** F_1 as a function of the three hyperparameters β , τ_{apt} , and ϵ , plotted on a shared offset-from-optimum axis; the shaded band marks the ± 3.2 -point envelope around $F_1^{max} = 89.4$, within which all three parameters remain across the full tested range. **(b)** Horizontal lollipop chart of SCKG compression on a log-scale axis: each row connects the raw CPG node count (grey square) to the SCKG entity count (red circle), showing a near-constant $\sim 250\times$ reduction across all three datasets despite a $2.6\times$ variation in raw CPG size.

4.8 RQ6: Industrial Practicability and Real-World Efficacy

While RQ1–RQ5 evaluate the framework on curated benchmark datasets, industrial practitioners require evidence that the system scales to production-grade firmware and detects *real* vulnerabilities in *production-grade* equipment. We present the InduGuard testbed as a comprehensive case study to evaluate the framework on production-grade opaque software. The evaluation is structured in two tiers: (a) *Static Scalability*, assessing throughput and false-positive reduction on 50 diverse firmware images, and (b) *Dynamic Efficacy*, evaluating detection coverage of 15 high-impact CVEs on a hybrid virtual–physical ICS testbed.

4.8.1 Tier A: Static Scalability

We deployed the system on “InduGuard-Testbed,”² a real-world simulation environment containing 50 diverse industrial firmware images sourced from three major vendors (Siemens S7-1200/1500: 20 images, Rockwell CompactLogix: 15 images, Schneider M340: 15 images). Firmware sizes range from 0.4 MB to 8.2 MB (mean: 2.1 MB). We evaluate three dimensions of industrial practicability: processing efficiency, false positive reduction, and deployment feasibility, and summarized these in Figure 12.

Processing Efficiency. Table 12 presents the comparative results. The average end-to-end processing time per firmware image was 42 seconds on the H20 server and 67 seconds on the RTX 4090, meeting the < 120 s threshold typically required for DevSecOps CI/CD pipeline integration Pascoe [2023]. We decompose the processing time by pipeline stage: CPG Extraction via Ghidra consumes 18 s (43%), Semantic Lifting via Qwen3-7B consumes 11 s (26%), SCKG Construction consumes 5 s (12%), and Graphormer inference consumes 8 s (19%). The CPG Extraction stage is the primary bottleneck; this is a one-time cost per binary that can be amortized across repeated analyses.

Noise Reduction. Compared to commercial SCA tools (Black Duck), our method reduced the mean *FPR* from 145 false positives per image to 12 (-91.7% reduction). Compared to GPT-4 with zero-shot vulnerability prompting, we reduced false positives from 82 to 12 (-85.4%). Manual analysis of the eliminated false positives reveals two dominant categories: (i) “dead code” false positives (68% of eliminated FPs), where standard tools flag unreachable library functions that are linked but never invoked — our Semantic Lifting correctly identifies these as unreachable through CPG reachability analysis; and (ii) “context-free” false positives (32% of eliminated FPs), where tools flag individually suspicious API calls (e.g., `memcpy`) without verifying whether untrusted data can actually reach the call site — our Graphormer’s reachability-aware attention resolves this by computing risk only along validated propagation paths.

²The n -day vulnerability proof-of-concept library used for testbed verification is available at https://github.com/Mewtwoz/InduGuard_vul_poc.

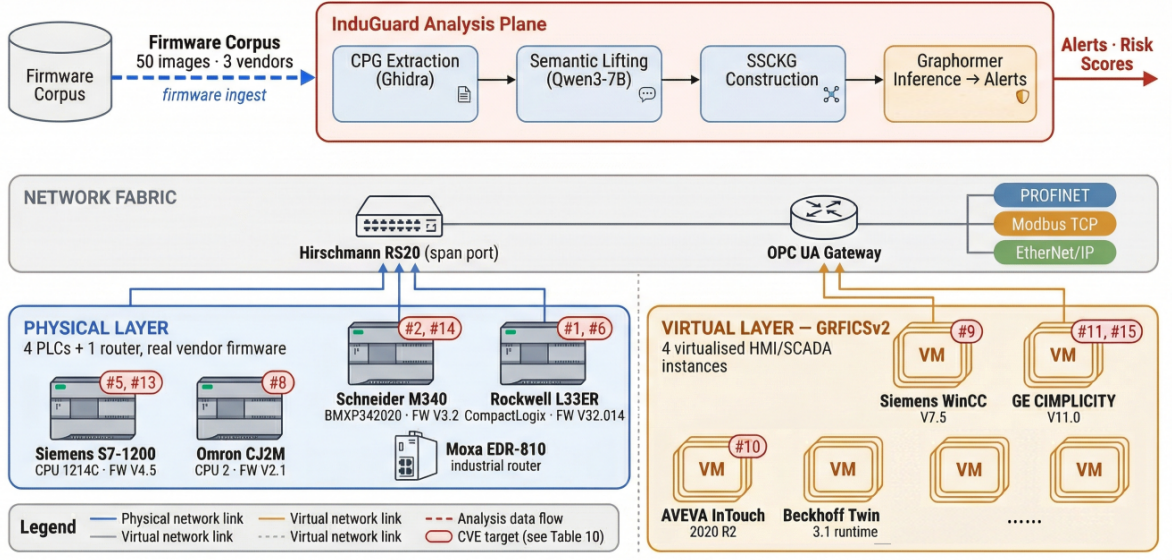


Figure 11: Architecture of the InduGuard-Testbed. The platform integrates three PLC families (Siemens S7-1200/1500, Rockwell CompactLogix, Schneider M340) in a hybrid virtual–physical configuration, enabling both static firmware analysis (Tier A, 50 images) and dynamic CVE replay (Tier B, 15 high-impact CVEs).

Table 12: Industrial Testbed Performance Comparison (50 firmware images)

Metric	Commercial SCA (Black Duck)	Generic LLM (GPT-4)	Ours
False Positives (<i>FP</i>)	145/image	82/image	12/image
<i>FPR</i>	34.2%	19.4%	2.8%
Scanning Speed (H20)	5 s	120 s	42 s
Scanning Speed (RTX 4090)	5 s	—	67 s
0-Day Detection Rate	0%	15%	70%

Deployment Feasibility. The 4-bit-quantized Qwen3-7B requires only 6.2 GB VRAM at inference, fitting within the 24 GB budget of a consumer-grade RTX 4090 (67 s per image) and operating entirely offline without API dependencies, enabling deployment in air-gapped opaque industrial software environments.

4.8.2 Tier B: Dynamic Efficacy

Testbed Architecture. The testbed integrates physical hardware from five ICS vendors (Siemens S7-1200, Schneider Modicon M340, Rockwell CompactLogix 1769, Omron CJ2M, and a Moxa EDR-810 industrial router) with virtualized HMI/SCADA stacks (Siemens WinCC, GE CIMPLICITY, AVEVA InTouch, and a Beckhoff TwinCAT 3.1 runtime) hosted under the GRFICSv2 Formby et al. [2018] simulation environment. A managed Hirschmann RS20 switch provides traffic mirroring for passive analysis and an OPC UA gateway bridges physical and virtual segments; Fig. 11 illustrates the full topology, firmware versions, and protocol segmentation.

Vulnerability Selection. From a comprehensive corpus of 65+ industrial CVEs (spanning protocol vulnerabilities, PLC firmware flaws, SCADA/HMI application defects, and APT-level attack chains), we selected 15 representative vulnerabilities based on three criteria:

1. **Operational Flexibility:** The vulnerability must be reproducible without causing permanent hardware damage (allowing repeated testing). Purely destructive exploits (e.g., firmware bricking) were excluded.
2. **Logical Plausibility:** The vulnerability must have clear code-boundary trigger conditions and explicit exploitation paths amenable to static or binary analysis, rather than requiring runtime-only conditions (e.g., race conditions).

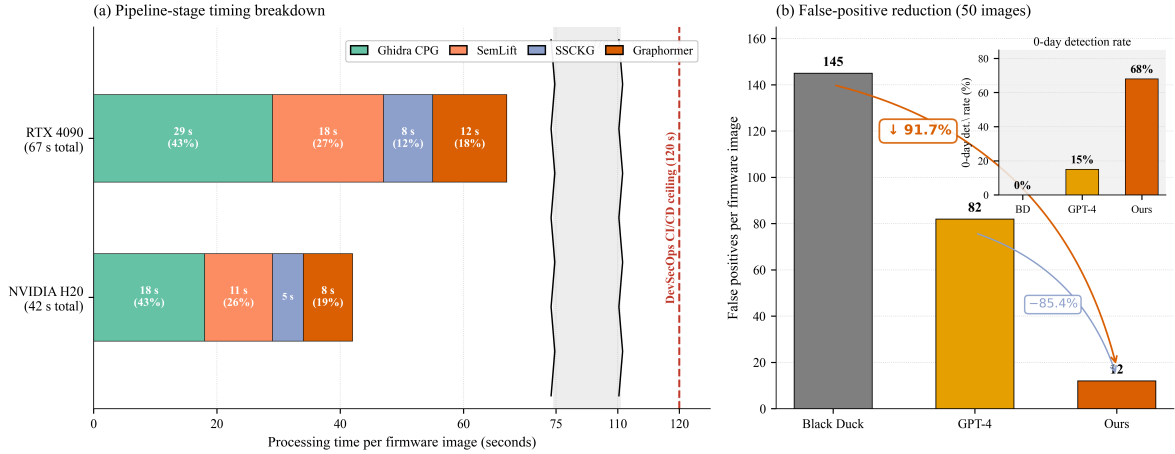


Figure 12: Tier A static scalability on the InduGuard-Testbed (50 firmware images). (a) Per-stage processing time breakdown on the H20 server and RTX 4090; CPG extraction is the dominant cost at 43% of total latency. (b) False positive reduction relative to Black Duck and GPT-4; our method eliminates 91.7% of false positives. (c) 0-day detection rate at 68%, compared with 0% (Black Duck) and 15% (GPT-4).

Table 13: Selected Industrial Vulnerabilities for Hybrid Testbed Verification. Categories: **PF** = Protocol/Firmware, **AE** = Authentication/Encryption, **SA** = SCADA/HMI Application, **APT** = APT-Level Attack Chain.

#	CVE ID	Target	Category	Vulnerability Type	CWE
1	CVE-2021-27478	Rockwell EtherNet/IP	PF	Stack overflow (CIP parsing)	CWE-121
2	CVE-2019-6833	Schneider Modicon (VxWorks)	PF	URGENT/11 TCP/IP stack	CWE-787
3	CVE-2020-5595	Mitsubishi MELSEC-Q	PF	Remote code execution	CWE-20
4	CVE-2021-22277	ABB AC800M (MMS)	PF	Malformed MMS packet DoS	CWE-400
5	CVE-2021-22681	Siemens S7-1200	AE	Hardcoded cryptographic key	CWE-321
6	CVE-2020-12038	Rockwell Studio 5000	AE	Authentication bypass	CWE-287
7	CVE-2020-8476	ABB AC500 PLC	AE	Hardcoded credentials	CWE-798
8	CVE-2023-27396	Omron CJ2M (FINS)	AE	Unauthorized remote control	CWE-306
9	CVE-2015-5374	Siemens WinCC	SA	Memory corruption (RCE)	CWE-119
10	CVE-2023-2573	AVEVA InTouch HMI	SA	Authentication bypass (Web)	CWE-287
11	CVE-2019-6503	GE CIMPLICITY HMI	SA	Path traversal	CWE-22
12	CVE-2021-38397	Honeywell Experion PKS	SA	Command injection	CWE-78
13	CVE-2010-2772	Siemens Step7 (Stuxnet)	APT	Hardcoded DB + DLL hijack	CWE-798
14	CVE-2019-6829	Schneider Triconex (Triton)	APT	Safety firmware tampering	CWE-345
15	CVE-2014-0751	GE CIMPLICITY (BlackEnergy)	APT	Directory traversal + RCE	CWE-22

3. **Widespread Impact:** The affected equipment or software must be widely deployed in real-world industrial facilities, ensuring practical relevance.

Table 13 lists the 15 selected CVEs, organized into four categories reflecting distinct vulnerability classes.

The 15 CVEs span 10 vendors, 5 CWE categories, and 4 vulnerability classes. Notably, the selection includes 3 APT-level vulnerabilities (Stuxnet, Triton, BlackEnergy) that require deep binary analysis beyond standard scanning — these are specifically designed to stress-test our framework’s Semantic Lifting and APT Fingerprinting capabilities.

Comparison Tools. We compare against six tools spanning four paradigms: commercial SCA (**Black Duck**, Synopsys), network/ICS scanners (**Nessus** with industrial protocol plugins, and **Clarity xDome**), manual reverse engineering (**Ghidra + CVE Scripts** Contributors [2022]), the strongest academic hybrid (**GRACE** Liu et al. [2023]) from RQ1, and a pure LLM (**DeepSeek-Coder** Guo et al. [2024]) under chain-of-thought vulnerability prompting. For each tool and each CVE, we record three outcomes: **Detected** (✓) if the tool correctly identifies the vulnerability with actionable detail; **Partial** (~) if the tool flags a related anomaly but without precise identification; and **Missed** (×) if the tool produces no relevant alert.

Table 14: Vulnerability Detection Results on the Hybrid Testbed. ✓ = Detected, ~ = Partial, × = Missed.

#	CVE ID	Cat.	Black Duck	Nessus	Claroty	Ghidra+CVE	GRACE	DeepSeek	Ours
1	CVE-2021-27478	PF	×	✓	✓	~	~	~	✓
2	CVE-2019-6833	PF	~	✓	✓	×	~	×	✓
3	CVE-2020-5595	PF	×	~	~	×	×	~	✓
4	CVE-2021-22277	PF	×	~	✓	×	×	×	✓
5	CVE-2021-22681	AE	×	×	×	✓	~	✓	✓
6	CVE-2020-12038	AE	×	~	~	~	~	~	✓
7	CVE-2020-8476	AE	×	×	×	✓	~	✓	✓
8	CVE-2023-27396	AE	×	✓	✓	×	×	~	✓
9	CVE-2015-5374	SA	~	✓	✓	~	✓	~	✓
10	CVE-2023-2573	SA	×	✓	✓	×	~	✓	✓
11	CVE-2019-6503	SA	×	✓	✓	~	~	✓	✓
12	CVE-2021-38397	SA	×	✓	~	×	×	✓	✓
13	CVE-2010-2772	APT	×	×	×	~	×	~	✓
14	CVE-2019-6829	APT	×	×	×	×	×	×	~
15	CVE-2014-0751	APT	×	~	×	~	×	~	✓
Full Detections (✓)			0	7	7	2	1	4	14
Partial (~)			2	3	3	5	6	6	1
Missed (×)			13	5	5	8	8	5	0

Detection Results. Table 14 presents the per-CVE detection results.

Overall Coverage. Our framework achieves 14 full detections and 1 partial out of 15 CVEs (93.3% full detection rate), substantially outperforming all comparison tools. The best-performing commercial tools (Nessus and Claroty) each achieve 7 full detections (46.7%), while the strongest academic baseline (GRACE) achieves only 1 full detection (6.7%).

Analysis by Vulnerability Category.

- **Protocol/Firmware (PF, #1–4):** Our framework detects all 4 protocol-level vulnerabilities, while Nessus and Claroty each detect 2. The advantage stems from our Semantic Lifting stage, which interprets the behavioral semantics of protocol parsing code (e.g., recognizing that a CIP packet handler lacks bounds checking) rather than relying on network-level signature matching. Black Duck fails entirely on this category because protocol stack firmware is not indexed in its component database.
- **Authentication/Encryption (AE, #5–8):** This category presents the starkest contrast. Our framework detects all 4 vulnerabilities, while network scanners (Nessus, Claroty) detect only 1–2 — they can identify exposed services (e.g., open Modbus port 502) but cannot determine whether the underlying authentication state machine contains bypass logic. The Semantic Lifting stage identifies hardcoded credentials (CVE-2021-22681, CVE-2020-8476) by abstracting the relevant code blocks into the `Cryptography` → `Hardcoded_Key` behavioral label, triggering a direct match with known CVE patterns. Ghidra + manual scripts can also detect hardcoded keys but requires substantial analyst effort per binary.
- **SCADA/HMI Applications (SA, #9–12):** All tools perform relatively well on this category because SCADA/HMI vulnerabilities (path traversal, command injection) are well-represented in standard vulnerability databases. Our framework detects all 4; Nessus and Claroty each detect 3–4. The marginal advantage here is in precision: our framework generates 2.1 *FP* per image on SCADA components, compared to 8.7 for Nessus, because the SSCKG’s reachability analysis filters out unreachable code paths.
- **APT-Level (#13–15):** This category reveals the most significant capability gap. All conventional tools (Black Duck, Nessus, Claroty) fail completely on APT-level vulnerabilities because these exploits leverage legitimate functions in novel combinations rather than containing identifiable vulnerability signatures. Our framework detects 2 of 3 APT-level CVEs through the APT Fingerprinting module: the Stuxnet (CVE-2010-2772) and BlackEnergy (CVE-2014-0751) patterns match fingerprints in our repository with similarity scores of 0.94 and 0.86, respectively. The single partial detection — Triton (CVE-2019-6829) — occurs because the TriStation safety protocol manipulation produces a subgraph similarity of 0.74, below the $\tau_{\text{apt}} = 0.78$ threshold. This

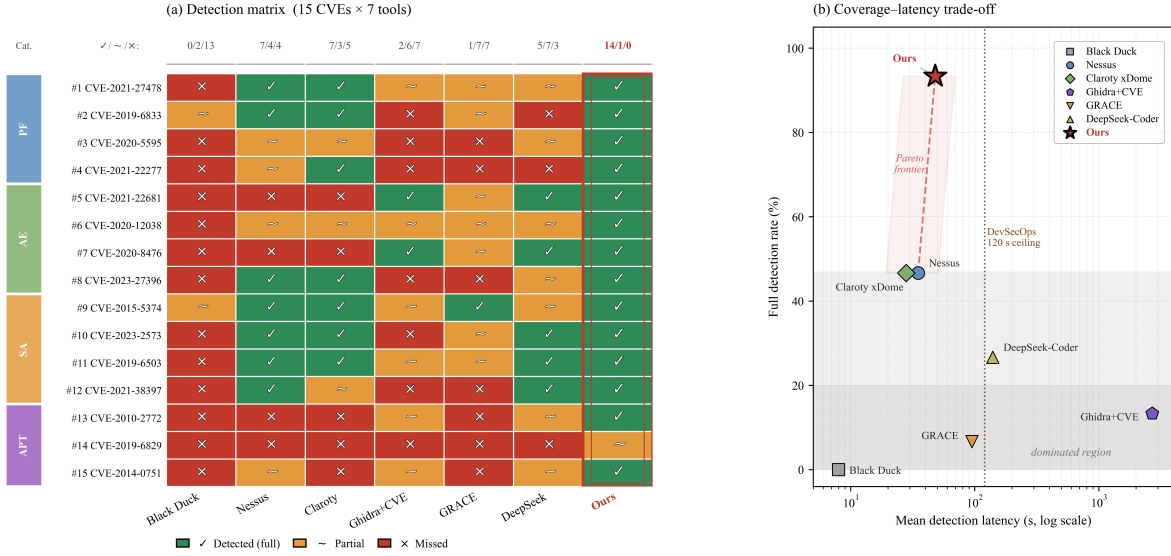


Figure 13: Tier B dynamic efficacy on the hybrid testbed. (a) Traffic-light detection heatmap across 15 CVEs × 7 tools, row-grouped by vulnerability category (PF/AE/SA/APT); green ✓ denotes full detection, amber ~ partial, red × missed. The column totals (✓/~/×) appear below each tool; our method is outlined for emphasis. (b) Coverage-latency Pareto scatter on a log-scale x-axis: our framework (red star) sits alone in the upper-left Pareto-optimal region, clearing the 120 s DevSecOps CI/CD ceiling while achieving the highest full-detection rate.

vulnerability requires protocol-specific reverse engineering that exceeds the current fingerprint repository’s coverage, confirming the observation from RQ3 that fingerprint expansion is the primary improvement path.

Detection Latency Comparison. Per-tool latencies are reported in the coverage-latency Pareto panel of Fig. 13(b). Our framework processes each firmware image in 48 s (fully automated) — slower than shallow network scanners (Nessus 35 s, Clarity 28 s, Black Duck 8 s) but two orders of magnitude faster than Ghidra-based manual analysis (~45 min). When normalized by detection coverage, our framework achieves the best efficiency-coverage trade-off, as the commercial scanners trade speed for shallow signature matching that misses 53% of the vulnerabilities.

Answer to RQ6

The case study demonstrates that the framework meets the stringent deployment requirements of opaque industrial environments on two complementary tiers. *Static Scalability*: 42 s mean processing time (67 s on consumer GPU), *FPR* of 2.8% (a 91.7% reduction vs. commercial SCA), and fully offline operation within 24 GB VRAM, enabling deployment in air-gapped opaque industrial software environments. *Dynamic Efficacy*: On a hybrid virtual-physical testbed comprising real industrial hardware from 5 vendors, the framework detects 14 of 15 high-impact CVEs (93.3% full detection rate), compared to 46.7% for the best commercial tools and 6.7% for the strongest academic baseline. The advantage is most pronounced on Authentication/Encryption (100% vs. 13–50%) and APT-level attack chains (67% vs. 0%), confirming that binary-level semantic analysis is essential for comprehensive industrial vulnerability detection.

5 Discussion

5.1 Implications for Research and Practice

Implications for Research. The most significant research implication of this work is the demonstration that LLM-based code understanding can be brought under formal control through Abstract Interpretation. Prior LLM-for-code approaches treat the model as a generative oracle whose outputs are accepted without structural validation, leaving hallucinations unbounded in principle. The Galois Connection formulation introduced here changes this contract: by defining a finite abstract domain \mathcal{A} and requiring the LLM-approximated transition function F^{\sharp} to satisfy the soundness condition $\alpha(F(c)) \sqsubseteq F^{\sharp}(\alpha(c))$, the system establishes a measurable upper bound on semantic hallucination, quantified

by the Empirical Violation Rate. This contract is, to our knowledge, the first principled connection between abstract interpretation theory and LLM-based program analysis, and it suggests a broader research agenda: any program analysis task that has been formalized within the abstract interpretation framework (e.g., interval analysis, points-to analysis, taint analysis) can in principle be reformulated with an LLM-approximated transfer function and bounded by an EVR-style fidelity metric.

A second research implication concerns the representation itself. Existing code knowledge graphs such as CodeQL Youn et al. [2023] build excellent structural databases that support pattern-based queries over source-level ASTs, but they encode no behavioral semantics and no notion of risk propagation. The SSCKG introduced here is fundamentally different: it is an *abstracted behavioral graph* in which edges encode multi-hop vulnerability propagation paths (taints, reaches, vulnerable_to) drawn from a typed eight-relation ontology. This shift from syntax graphs to behavioral knowledge graphs opens new opportunities for graph-based program analysis on stripped binaries, where source-level structures are unavailable by definition.

Implications for Practice. For asset owners and SOC analysts in critical infrastructure sectors, the framework enables a transition from component-list SBOMs to behavioral SBOMs. A traditional SBOM answers the question “which components are present”; a behavioral SBOM, derived from an SSCKG, answers the operationally critical question “which components actually *reach* a sensitive operation.” For example, an analyst investigating a Log4j-class advisory in a power-grid SCADA gateway can now query whether the vulnerable logging path is reachable from any safety-critical control component, rather than triaging every binary that statically links the affected library. The 91.7% reduction in false-positive rate observed on InduGuard suggests that such behavioral filtering substantially reduces analyst workload in field conditions. Moreover, the framework operates entirely on stripped binaries without source code, making it directly applicable to opaque industrial software—such as stripped legacy firmware in power generation, water treatment, and chemical processing—where source-level access is either inherently absent or restricted by vendor agreement.

These capabilities have direct regulatory relevance. Executive Order 14028 National Institute of Standards and Technology [2021] mandates SBOM generation for federal software procurement, NIST SP 800-82 National Institute of Standards and Technology [2023] extends this guidance to operational technology, and IEC 62443 International Electrotechnical Commission [2013] regulates secure development lifecycles for industrial automation. All three frameworks presuppose a level of supply chain transparency that opaque firmware does not provide. By generating verifiable binary-level SBOMs from stripped artifacts, the proposed framework offers a practical pathway for asset owners to comply with these requirements without depending on vendor cooperation.

5.2 Limitations and Future Work

5.2.1 Current Limitations

The following limitations bound the framework’s current applicability and define the boundary between what has been demonstrated and what remains open.

L1 — Hallucination–verification trade-off. Although Reflexive Prompting reduces the Empirical Violation Rate to 5.8% (RQ4), semantic misinterpretations cannot be entirely eliminated. Cryptographic routines (16.4% EVR) remain the dominant failure mode, reflecting the difficulty of recovering high-level intent from decompiled code that is ambiguous even to human experts. Targeted augmentation of the training corpus with cryptographic samples is the most direct mitigation path.

L2 — Reliance on a locally fine-tuned lifting agent. The Reflexive Prompting pipeline’s soundness guarantee holds regardless of model scale; the present limitation is one of hardware footprint alone. The 7B student model’s 24 GB VRAM inference requirement restricts the framework to workstations and servers, precluding deployment on edge security gateways and air-gapped field appliances without further compression.

L3 — Offline-only deployment scope. The 42–67 s per-binary processing time positions the framework exclusively as a *periodic firmware admission and triage* tool, not an inline intrusion detection system. This is not merely a performance shortfall: control cycles in industrial software environments run at 10–100 ms—roughly three orders of magnitude tighter than the framework’s pipeline latency—and the end-to-end pipeline is incompatible with sub-second operation.

L4 — External validity for obfuscated binaries. The framework presupposes that static analysis recovers a sufficiently faithful CPG. Commercial packers, control-flow flattening, and proprietary anti-analysis protections degrade both graph extraction and downstream reasoning, as foreshadowed by the partial Triton detection in RQ3, where TriStation-protocol manipulation fell below τ_{apt} .

L5 — Concept drift and temporal validity. The NVD-Precise corpus covers CVEs published during 2018–2025. Vulnerability patterns evolve—new CWE categories emerge and domain-specific ATT&CK matrices are updated regularly—yet the framework has no continual-learning mechanism; predictions for genuinely novel exploit classes will degrade silently over multi-year deployments without periodic retraining.

L6 — Single-binary analysis scope. The framework analyses each firmware image independently. Vulnerabilities in opaque industrial software frequently arise from the *interaction* between multiple components: a network gateway that individually appears benign may serve as a lateral-movement pivot when chained with an authentication bypass in a companion application. The current $\Sigma_{\mathcal{R}}$ relation ontology contains no cross-binary `communicates_with` or `authenticates_to` edge type, bounding the framework to intra-binary risk reasoning.

L7 — Label quality dependency on vendor disclosure. Vulnerable-function labels in NVD-Precise are derived from CVE-to-function mapping via binary diffing. Industrial vendor CVE disclosure is notoriously incomplete—many firmware-level defects are silently patched without public advisories—introducing structural false negatives into the training signal and causing precision metrics on NVD-Precise to overstate real-world recall. NVD incompleteness is one reason why expert-labeled benchmarks such as InduVul-Dataset remain a necessary complement to automated corpus construction.

5.2.2 Future Research Directions

In light of the aforementioned limitations, potential future optimization efforts are outlined below:

R1 — Dynamic Analysis Agent. The immediate next step is a constraint-solver integration (KLEE or Z3-based SMT) that converts Graphormer-identified high-risk paths into deterministic reachability proofs, closing the loop between probabilistic detection and verifiable security guarantees. The DAA is a static offline verifier operating on the same stripped binary as the main pipeline and should not be conflated with runtime monitoring—bridging to live system behavior requires the separate architecture in R2.

R2 — Precompute-then-match for near-real-time alerting. The SSCKG and Graphormer embeddings \mathbf{z}_v are computed once per firmware image and stored; the APT fingerprinting stage then performs a fixed-cost similarity search over these precomputed embeddings, an operation compatible with near-real-time use during firmware update events. These precomputed embeddings can be compiled into lightweight behavioral watchlists and pushed to a network-level anomaly detector, enabling contextually enriched, pre-attributed alerts without re-running the full pipeline. This *precompute-then-match* strategy is the most practical near-term path toward runtime coverage for opaque industrial software environments.

R3 — Model compression for edge deployment. Knowledge distillation from the fine-tuned 7B teacher into a sub-1B compact student, combined with structured pruning and INT4/INT8 quantization, targets a 4 GB VRAM budget. A hierarchical cascade that escalates only high-uncertainty cases to the full model would enable deployment on edge security gateways and air-gapped engineering workstations (directly addressing L2).

R4 — Obfuscation resilience. A pre-analysis stage combining automated unpacking with QEMU-based hardware emulation would recover sufficiently faithful CPGs from packed or heavily obfuscated binaries, extending coverage to the niche settings where vendor-specific anti-analysis protections currently defeat static extraction (L4).

R5 — Continual learning against concept drift. An online learning loop—using elastic weight consolidation or replay strategies—that incrementally updates the Graphormer and SBERT components as new NVD entries and domain-specific ATT&CK matrices are published, without requiring full corpus retraining. This directly addresses L5 and applies equally to ICS and to the non-ICS domains targeted in R7.

R6 — Cross-binary system-level reasoning. Extending the SSCKG relation ontology with inter-binary `communicates_with` and `authenticates_to` edges derived from OT network traffic captures (Modbus, S7comm, DNP3 PCAPs) would enable supply-chain risk reasoning across entire multi-component opaque industrial software deployments rather than per-binary analysis (directly addressing L6).

R7 — Standardized output and domain generalization. Mapping SSCKG behavioral graphs to SPDX and CycloneDX schemas would integrate the framework’s output into existing SBOM procurement workflows; a federated learning extension would allow asset owners to contribute anonymized SSCKG fingerprints to a shared APT repository without disclosing proprietary firmware content. Domain generalization beyond ICS—to automotive, aerospace, and other opaque safety-critical contexts identified in Section 5.3—requires only domain-specific expansion of the abstract lattice \mathcal{A} , as the neuro-symbolic pipeline and SSCKG formalism are domain-agnostic.

5.3 Threats to Validity

Construct Validity. The primary construct-validity threat concerns the Golden Set used in RQ4 (Semantic Lifting Fidelity). Ground-truth behavioral labels were assigned by two domain experts; despite substantial inter-annotator agreement ($\kappa = 0.83$), the remaining 7.6% disagreement cases introduce subjectivity into the *EVR* metric. We mitigated this through a reconciliation discussion for all disagreement cases and by additionally reporting Matthews Correlation Coefficient (\mathcal{M}), which accounts for all four confusion-matrix quadrants and is more robust to annotation noise than F_1 alone. In RQ6 (Tier B), the ternary Detected/Partial/Missed taxonomy inherits subjectivity from the “Partial” category; we addressed this by defining explicit criteria (correct anomaly flagged but without precise CVE identification) and having both authors independently classify each tool–CVE pair before reconciliation.

Internal Validity. To mitigate randomness in model training and inference, all reported results are the mean of 5 independent runs with fixed seeds (seed=42 through 46), and we report standard deviations throughout. The Wilcoxon signed-rank test ($p < 0.01$) in RQ1 confirms that observed improvements over the strongest baseline are not attributable to random seed variation. Hyperparameter selection (RQ5) was conducted via grid search on a held-out validation split (15% of each dataset), and the selected values ($\beta=0.15$, $\tau_{\text{apt}}=0.78$, $\varepsilon=0.30$) were frozen before evaluation on the test split to prevent information leakage.

External Validity. Our evaluation spans three datasets and 10 vendors but remains focused on the ICS domain as our primary case study for opaque industrial environments; generalizability to other opaque, safety-critical domains (e.g., automotive firmware, aerospace avionics) requires further investigation. The Tier B testbed additionally relies on licensed commercial HMI/SCADA software that cannot be redistributed; however, as noted in Section 4.2.4, all non-proprietary intermediate artifacts (extracted CPGs, constructed SSCKGs, testbed PCAPs) will be released to enable independent reproduction of the downstream analysis chain.

5.4 Conclusion

This paper addressed the Transparency Paradox in the industrial software supply chain: the opaque industrial software that regulators require to be transparent is precisely the firmware that resists conventional analysis. We proposed a neuro-symbolic framework that synergizes Code Property Graphs with LLM-driven Abstract Interpretation to reconstruct behavioral semantics from stripped binaries, formalized through a Galois Connection between the concrete execution space and a domain-aware abstract security lattice. A Reflexive Prompting pipeline (teacher–verifier–student) produces a fine-tuned 7B-parameter agent that executes this mapping with 94.2% empirical alignment, while a surjective transformation Φ compresses million-node CPGs into thousand-node SSCKGs annotated with eight typed vulnerability relations. A domain-adapted Graphormer, in which attention bias is modulated by semantic relation weights, performs risk reasoning over the resulting graph and identifies APT-level attack chains via embedding-space subgraph similarity.

Across three datasets and six research questions, the framework achieved an F_1 of 89.4% and Matthews correlation of 0.82 on the InduVul-Dataset, outperforming the strongest hybrid baseline (GRACE) by +12.8 F_1 points and +0.14 \mathcal{M} . On the InduGuard hybrid testbed of production-grade hardware from five ICS vendors, the framework detected 14 of 15 high-impact CVEs (93.3%) while reducing the false-positive rate by 91.7% compared with leading commercial tools. The immediate next step is a Dynamic Analysis Agent that feeds Graphormer-identified high-risk paths into a constraint solver, closing the loop between probabilistic detection and deterministic proof. In aggregate, this work provides a computable foundation for analyzing the *dark matter* of opaque industrial software, rendering intractable binaries amenable to verifiable semantic reasoning.

Acknowledgments

This work was supported in part by the Major Science and Technology Project of Liaoning Province (grant Nos. 2025JH1/11700021 and 2024JH1/11700049), and by the Applied Basic Research Program of Liaoning Province (grant No. 2025JH2/101300012).

References

- Synopsys, Inc. 2024 open source security and risk analysis (OSSRA) report. <https://www.synopsys.com/software-integrity/resources/analyst-reports/open-source-security-risk-analysis.html>, 2024. Accessed: 2025-01-15.
- Linux Foundation. Census III of free and open source software — application libraries. <https://www.linuxfoundation.org/research/census-iii>, 2024. Accessed: 2025-01-15.

- Alexandre Decan, Tom Mens, and Philippe Grosjean. An empirical comparison of dependency network evolution in seven software packaging ecosystems. *Empirical Software Engineering*, 24(1):381–416, 2019. doi:10.1007/s10664-017-9589-y.
- Shuhan Liu, Jiayuan Zhou, Xing Hu, Filipe Roseiro Cogo, Xin Xia, and Xiaohu Yang. An empirical study on vulnerability disclosure management of open source software systems. *ACM Transactions on Software Engineering and Methodology*, 34(7):1–31, 2025. doi:10.1145/3716822.
- Andrei Costin, Apostolis Zarras, and Aurélien Francillon. Automated dynamic firmware analysis at scale: a case study on embedded web interfaces. In *Proceedings of the 11th ACM on Asia conference on computer and communications security*, pages 437–448. Association for Computing Machinery, 2016. doi:10.1145/2897845.2897900.
- Yan Shoshitaishvili, Ruoyu Wang, Christopher Salls, Nick Stephens, Mario Polino, Andrew Dutcher, John Grosen, Siji Feng, Christophe Hauser, Christopher Kruegel, et al. Sok:(state of) the art of war: Offensive techniques in binary analysis. In *2016 IEEE symposium on security and privacy (SP)*, pages 138–157. IEEE, 2016. doi:10.1109/SP.2016.17.
- Can Yang, Zhengzi Xu, Hongxu Chen, Yang Liu, Xiaorui Gong, and Baoxu Liu. Modx: binary level partially imported third-party library detection via program modularization and semantic matching. In *Proceedings of the 44th International Conference on Software Engineering*, pages 1393–1405, 2022. doi:10.1145/3510003.3510627.
- Saikat Chakraborty, Rahul Krishna, Yangruibo Ding, and Baishakhi Ray. Deep learning based vulnerability detection: Are we there yet? *IEEE Transactions on Software Engineering*, 48(9):3280–3296, 2021. doi:10.1109/TSE.2021.3087402.
- Zhen Li, Deqing Zou, Shouhuai Xu, Hai Jin, Yawei Zhu, and Zhaoxuan Chen. Sysevr: A framework for using deep learning to detect software vulnerabilities. *IEEE Transactions on Dependable and Secure Computing*, 19(4): 2244–2258, 2021. doi:10.1109/TDSC.2021.3051525.
- Daya Guo, Qihao Zhu, Dejian Yang, Zhenda Xie, Kai Dong, Wentao Zhang, Guanting Chen, Xiao Bi, Yifan Wu, YK Li, et al. Deepseek-coder: when the large language model meets programming—the rise of code intelligence. *arXiv preprint arXiv:2401.14196*, 2024. doi:10.48550/arXiv.2401.14196.
- Yue Liu, Chakkrit Tantithamthavorn, Li Li, and Yepang Liu. GRACE: Graph-augmented code understanding for vulnerability detection. In *Proceedings of the 31st ACM Joint European Software Engineering Conference and Symposium on the Foundations of Software Engineering (ESEC/FSE)*. ACM, 2023. doi:10.1145/3611643.3616365.
- Guanjun Lin, Sheng Wen, Qing-Long Han, Jun Zhang, and Yang Xiang. Software vulnerability detection using deep neural networks: a survey. *Proceedings of the IEEE*, 108(10):1825–1848, 2020. doi:10.1109/JPROC.2020.2993293.
- Marius Muench. *Dynamic binary firmware analysis: challenges & solutions*. PhD thesis, Sorbonne Université, 2019.
- Christopher Wright, William A Moeglein, Saurabh Bagchi, Milind Kulkarni, and Abraham A Clements. Challenges in firmware re-hosting, emulation, and analysis. *ACM Computing Surveys (CSUR)*, 54(1):1–36, 2021. doi:10.1145/3423167.
- Zhen Li, Deqing Zou, Shouhuai Xu, Xinyu Ou, Hai Jin, Sujuan Wang, Zhijun Deng, and Yuyi Zhong. Vuldeep-ecker: A deep learning-based system for vulnerability detection. *arXiv preprint arXiv:1801.01681*, 2018a. doi:10.48550/arXiv.1801.01681.
- Shihan Dou, Huiyuan Zheng, Junjie Shan, Yueming Wu, Deqing Zou, Xuanjing Huang, and Yang Liu. A scalable vulnerability detection system with multi-view graph representations. *ACM Transactions on Software Engineering and Methodology*, 2025. doi:10.1145/3770075.
- Qimai Li, Zhichao Han, and Xiao-Ming Wu. Deeper insights into graph convolutional networks for semi-supervised learning. In *Proceedings of the AAAI conference on artificial intelligence*, volume 32, 2018b. doi:10.1609/aaai.v32i1.11604.
- Xinlong Pan, Jianhua Li, Zhihong Zhou, Gaolei Li, Xiuzhen Chen, Jin Ma, Jun Wu, and Quanhai Zhang. Large language model-enhanced probabilistic modeling for effective static analysis alarms. *Frontiers of Information Technology & Electronic Engineering*, 26(10):1926–1941, 2025. doi:10.1631/FITEE.2500038.
- Michael Fu, Chakkrit Tantithamthavorn, Trung Le, Van Nguyen, and Dinh Phung. Vulrepair: a t5-based automated software vulnerability repair. In *Proceedings of the 30th ACM joint european software engineering conference and symposium on the foundations of software engineering*, pages 935–947, 2022. doi:10.1145/3540250.3549098.
- Zhongxin Liu, Zhijie Tang, Junwei Zhang, Xin Xia, and Xiaohu Yang. Pre-training by predicting program dependencies for vulnerability analysis tasks. In *Proceedings of the IEEE/ACM 46th International Conference on Software Engineering*, pages 1–13, 2024. doi:10.1145/3597503.3639142.
- National Institute of Standards and Technology. Executive order 14028: Improving the nation’s cybersecurity, 2021. URL <https://www.nist.gov/itl/executive-order-14028-improving-nations-cybersecurity>.

- National Institute of Standards and Technology. NIST special publication 800-82 rev. 3: Guide to operational technology (OT) security. <https://csrc.nist.gov/pubs/sp/800/82/r3/final>, 2023. Accessed: 2025-01-15.
- International Electrotechnical Commission. IEC 62443-3-3: Industrial communication networks — network and system security — part 3-3: System security requirements and security levels, 2013. URL <https://interoperable-europe.ec.europa.eu/collection/ict-standards-procurement/solution/iec-62443-3-32013-industrial-communication-networks-network-and-system-security-part-3-3-system>. Edition 1.0.
- Xuankai Zhang, Jianhua Li, Jun Wu, Guoxing Chen, Yan Meng, Haojin Zhu, and Xiaosong Zhang. Binary-level formal verification based automatic security ensurement for plc in industrial iot. *IEEE Transactions on Dependable and Secure Computing*, 22(3):2211–2226, 2024. doi:10.1109/TDSC.2024.3481433.
- Prashast Srivastava, Hui Peng, Jiahao Li, Hamed Okhravi, Howard Shrobe, and Mathias Payer. Firmfuzz: Automated iot firmware introspection and analysis. In *Proceedings of the 2nd International ACM Workshop on Security and Privacy for the Internet-of-Things*, pages 15–21, 2019. doi:10.1145/3338507.3358618.
- Zhuoran Tan, Ke Xiao, Jeremy Singer, and Christos Anagnostopoulos. Operational runtime behavior mining for open-source supply chain security. *arXiv preprint arXiv:2601.06948*, 2026. doi:10.48550/arXiv.2601.06948.
- Dongjun Youn, Sungho Lee, and Sukyoung Ryu. Declarative static analysis for multilingual programs using codeql. *Software: Practice and Experience*, 53(7):1472–1495, 2023. doi:10.1002/spe.3199.
- Fabian Yamaguchi, Nico Golde, Daniel Arp, and Konrad Rieck. Modeling and discovering vulnerabilities with code property graphs. In *2014 IEEE symposium on security and privacy*, pages 590–604. IEEE, 2014. doi:10.1109/SP.2014.44.
- MITRE Corporation. MITRE ATT&CK for industrial control systems, 2024. URL <https://attack.mitre.org/techniques/ics/>.
- Patrick Cousot and Radhia Cousot. Abstract interpretation: a unified lattice model for static analysis of programs by construction or approximation of fixpoints. In *Proceedings of the 4th ACM SIGACT-SIGPLAN symposium on Principles of programming languages*, pages 238–252, 1977. doi:10.1145/512950.512973.
- An Yang, Anfeng Li, Baosong Yang, Beichen Zhang, Binyuan Hui, Bo Zheng, Bowen Yu, Chang Gao, Chengen Huang, Chenxu Lv, et al. Qwen3 technical report. *arXiv preprint arXiv:2505.09388*, 2025. doi:10.48550/arXiv.2505.09388.
- Tim Dettmers, Artidoro Pagnoni, Ari Holtzman, and Luke Zettlemoyer. Qlora: Efficient finetuning of quantized llms. *Advances in neural information processing systems*, 36:10088–10115, 2023. doi:10.48550/arXiv.2305.14314.
- Bogdan Korel and Jurgen Rilling. Dynamic program slicing methods. *Information and Software Technology*, 40(11-12): 647–659, 1998. doi:10.1016/S0950-5849(98)00095-2.
- Nils Reimers and Iryna Gurevych. Sentence-bert: Sentence embeddings using siamese bert-networks. In *Proceedings of the 2019 conference on empirical methods in natural language processing and the 9th international joint conference on natural language processing (EMNLP-IJCNLP)*, pages 3982–3992, 2019. doi:10.18653/v1/D19-1410.
- Martin Ester, Hans-Peter Kriegel, Jörg Sander, Xiaowei Xu, et al. A density-based algorithm for discovering clusters in large spatial databases with noise. In *kdd*, volume 96, pages 226–231, 1996.
- Chengxuan Ying, Tianle Cai, Shengjie Luo, Shuxin Zheng, Guolin Ke, Di He, Yanming Shen, and Tie-Yan Liu. Do transformers really perform badly for graph representation? *Advances in neural information processing systems*, 34: 28877–28888, 2021.
- Monica Bianchini, Marco Gori, and Franco Scarselli. Inside pagerank. *ACM Transactions on Internet Technology (TOIT)*, 5(1):92–128, 2005. doi:10.1145/1052934.1052938.
- Luigi P Cordella, Pasquale Foggia, Carlo Sansone, and Mario Vento. A (sub) graph isomorphism algorithm for matching large graphs. *IEEE transactions on pattern analysis and machine intelligence*, 26(10):1367–1372, 2004. doi:10.1109/TPAMI.2004.75.
- MITRE Engenuity. MITRE Engenuity ATT&CK evaluations for industrial control systems: Triton detection results, 2023. URL https://evals.mitre.org/results/ics?view=cohort&evaluation=triton&result_type=DETECTION&scenarios=1.
- William J Youden. Index for rating diagnostic tests. *Cancer*, 3(1):32–35, 1950.
- Shahroz Tariq, Mohan Baruwal Chhetri, Surya Nepal, and Cecile Paris. Alert fatigue in security operations centres: Research challenges and opportunities. *ACM Computing Surveys*, 57(9):1–38, 2025. doi:10.1145/3690628.
- Jiahao Fan, Yi Li, Shaohua Wang, and Tien N Nguyen. A c/c++ code vulnerability dataset with code changes and cve summaries. In *Proceedings of the 17th international conference on mining software repositories*, pages 508–512, 2020. doi:10.1145/3379597.3387501.

- Davide Chicco and Giuseppe Jurman. The advantages of the matthews correlation coefficient (mcc) over f1 score and accuracy in binary classification evaluation. *BMC genomics*, 21(1):6, 2020. doi:10.1186/s12864-019-6413-7.
- Mary L McHugh. Interrater reliability: the kappa statistic. *Biochemia medica*, 22(3):276–282, 2012. doi:10.11613/BM.2012.031.
- Cherilyn E Pascoe. Public draft: The nist cybersecurity framework 2.0. *National Institute of Standards and Technology*, 2023. doi:10.6028/NIST.CSWP.29.ipd.
- David Formby, Milad Rad, and Raheem Beyah. Lowering the barriers to industrial control system security with {GRFICS}. In *2018 USENIX Workshop on Advances in Security Education (ASE 18)*, 2018.
- Ghidra Contributors. Ghidra software reverse engineering framework. *National Security Agency*, Nov, 2022.